AD-A261 200

MENTATION PAGE

Form Approved
OMB No 0704-0188

1. AGENCY USE ONLY (Leave blank)	2. REPORT DATE	3. REPORT TYPE AND DATES COVERED
	Feb. 1993	Annual Letter Fiscal 1992

4. TITLE AND SUBTITLE
The Effects of Raman Scattering Across the Visible Spectrum in Clear Ocean Water: A Monte Carlo Study

5. FUNDING NUMBERS
G
N00014-89-J-3137/
P00003

6. AUTHOR(S)

Robert H. Stavn

7. PERFORMING ORGANIZATION NAME(S) AND ADDRESS(ES)

Dept. of Biology
Univ. of North Carolina/Greensboro
Greensboro, NC 27412

8. PERFORMING ORGANIZATION REPORT NUMBER

9. SPONSORING/MONITORING AGENCY NAME(S) AND ADDRESS(ES)
Office of Naval Research
Ocean Science Directorate
Ocean Optics Division
800 N. Quincy Street
Arlington, VA 22217-5000

10. SPONSORING/MONITORING AGENCY REPORT NUMBER

11. SUPPLEMENTARY NOTES

Approved for Public Release: Distribution unlimited

12a. DISTRIBUTION/AVAILABILITY STATEMENT

To be published in Applied Optics

13. ABSTRACT (Maximum 200 words)

This report documents the effects of water Raman scattering activity in clear ocean waters for the visible spectrum. The mode of study is a Monte Carlo simultion utilizing the accepted physical properties of the water molecule and minimal amounts of suspended matter. This Raman scattering activity has a significant effect on the upwelling irradiance in air and on the properties of the sumbarine light field in the surface layers. At wavelengths greater than 500 nm the water Raman activity significantly affects the submarine light field at depth.

14. SUBJECT TERMS	15. NUMBER OF PAGES
water Raman scattering, ocean optics, remote sensing reflectance	64
	16. PRICE CODE

17. SECURITY CLASSIFICATION OF REPORT	18. SECURITY CLASSIFICATION OF THIS PAGE	19. SECURITY CLASSIFICATION OF ABSTRACT	20. LIMITATION OF ABSTRACT
UNCLASSIFIED	UNCLASSIFIED	UNCLASSIFIED	

NSN 7540-01-280-5500

Standard Form 298 (Rev 2-89)
Prescribed by ANSI Std 239-18
298-102

THE EFFECTS OF RAMAN SCATTERING ACROSS THE VISIBLE SPECTRUM IN CLEAR OCEAN WATER: A MONTE CARLO STUDY

Robert Hans Stavn
University of North Carolina/Greensboro
Department of Biology
Greensboro, NC 27412

ABSTRACT

Raman scattering activity in clear ocean waters is documented for the entire visible spectrum from Monte Carlo simulations. The Raman scattering activity has a significant effect on the upwelling irradiance value in air and on the submarine light field at the water surface over the entire visible spectrum. A reduction in Raman scattering activity at 440 nm due to Fraunhofer lines at the Raman source wavelengths is also demonstrated. At wavelengths greater than 500 nm Raman scattering makes a significant contribution to the in-water light field at depth.

KEY WORDS

Raman scattering, ocean optics, remote sensing reflectance, in-water optical properties, Fraunhofer lines

I. Introduction

The reality of the occurrence of water Raman scattering in clear ocean waters has been established by Stavn and Weidemann[1,2] and Marshall and Smith[3,4] after the strong implications of its presence were reported by Sugihara et al.[5] Stavn and Weidemann utilized field results and Monte Carlo simulations of the radiative transfer equation to establish the water Raman scattering phenomenon at 520 nm, while Marshall and Smith used field results and a modified two-flow model to establish it at 589 nm.

In studies of ocean optics, it has long been recognized that there is a need for accurate information on the absorption and scattering characteristics of the water molecule. This information provides a baseline to evaluate field measurements of ocean optical properties, make radiative transfer predictions, calculate photon budgets, etc. To these ends there is now developing a need for accurate information on the transpectral scattering properties of the water molecule. This Raman scattering phenomenon results from the thermal vibrational properties of the water molecule in which energy can be abstracted from a photon to put the molecule into a specific vibrational mode of OH stretching and bending.[6] The photon is then emitted at a longer wavelength in this Stokesian mode.

Anti-Stokesian modes are also possible but of very low probability at the ambient temperatures of the world ocean.

The next question for clear ocean waters, after water Raman activity in the region of 520 - 589 nm has been established, is whether the water Raman scattering phenomenon is significant for the shorter (blue) and longer (red) wavelengths of the visible spectrum. Certainly the insolation of the sea surface is rich in the blue and ultraviolet wavelengths, especially in the surface layers. There is concern also about possible increases in the UV portion of the insolation from reduction in the ozone layer.[7] Water Raman scattering follows a λ^{-4} law and thus there would be relatively greater production of water Raman photons at shorter wavelengths. We have at least the potential of significant effects at shorter wavelengths. This same law would imply relatively fewer water Raman photons at longer wavelengths, and we want to see if the phenomenon can be as significant as the fluorescence of chlorophyll, for example. Many remote sensing algorithms require a region in the red (about 670 nm) where the water leaving radiance or irradiance is essentially zero.[8] The possibility of water Raman scattering activity here is certainly relevant.

The present work uses the Monte Carlo simulation of the radiative transfer equation as a "controlled experiment" in observing the photon penetration of the clear, oligotrophic ocean

as has been stated by Gordon.[9] The validity of the simulation method has been established from comparison of Monte Carlo output with actual ocean data.[1,2] Fundamental baselines of Raman scattering activity across the entire visible spectrum are needed for evaluation and interpretation of remote sensing algorithms, models of photon penetration, etc. Fluorescence, at first recognized as a phenomenon of chlorophyll *a* at about 685 nm,[10] is now observed from other intracellular pigments at several wavelengths[11] and from dissolved organic matter.[12,13] Thus a water Raman baseline is needed to evaluate the importance of fluorescence from the previously mentioned sources in the oceanic radiation field. Certainly, the Raman scattering phenomenon has been used for a long time to normalize the fluorescence signals received from active remote sensing by LIDAR.[14] And the ongoing attempts to invert the inherent optical properties of the marine hydrosol from the irradiance field require a knowledge of the contribution of water Raman scattering. These needs can be met with the Monte Carlo simulations of the NOARL optical model. With the input of the recognized optical parameters of the marine hydrosol, the NOARL optical model can generate separate solar and water Raman photon streams for analysis. Combining the separate photon streams then gives us insight into the effects of water Raman scattering on the submarine light field.

II. Methods

The NOARL optical model is a Monte Carlo simulation of the radiative transfer equation which describes the penetration of solar photons into ocean waters. It also accounts for the transpectral water Raman scattering. This Monte Carlo simulation is derived from the methods of Plass and Kattawar,[15] Gordon and Brown[16] and Kirk.[17] The required inputs for simulating the penetration and fate of solar photons in ocean waters are the absorption coefficient, total scattering coefficient, and the volume scattering function of the marine hydrosol. The volume scattering functions of each scattering component (molecular water, quartz-like particulates, algae, organic detritus) are treated separately rather than using an average volume scattering function. The NOARL Blue Water Model used in this simulation contains the absorption coefficients for molecular water reported by Smith and Baker[18] up to 570 nm; the coefficients reported by Tam and Patel[19] are used at wavelengths greater than 570 nm. Recent investigations of the backscattered upwelling radiance from ocean waters indicate that this is the most efficient combination of absorption coefficients.[20] The total scattering coefficient and the volume scattering function of pure seawater are incorporated from Morel,[21] the total scattering coefficient for quartz-like material is from Kullenberg,[22] and the volume

scattering function is incorporated from the Petzold[23] AUTEC distribution corrected for molecular water.[21] There are no other hydrosol components assumed in the Blue Water Model.

To simulate the genesis and fate of the photons transpectrally scattered from the water molecule, its Raman scattering coefficient was calculated from the molecular Raman scattering cross section reported by Marshall and Smith[4] and from the depolarization ratios reported by Murphy and Bernstein.[24] The Raman scattering coefficient was then truncated to generate only emissions in the 10 nm waveband surrounding the emission wavelength studied, as described earlier.[1] Since the frequency shift of water Raman emission from a line source at any wavelength occurs approximately in the range 2900 cm^{-1} to 3700 cm^{-1}, it is practical and convenient to divide the relatively broad Raman emission band into three bands of 10 nm bandwidth: a mid-band, an upper-band, and a lower-band. The emission in the mid-band will dominate at shorter wavelengths and more emission is distributed among the upper and lower bands at longer wavelengths. The mid-band represents a frequency shift centered at approximately 3357 cm^{-1},[5] the upper band represents a frequency shift centered at approximately 3500 cm^{-1}, and the lower band represents a frequency shift centered at approximately 3150 cm^{-1}.

The primary source waveband for the water Raman emissions at

a given waveband is determined by calculation based on the 3357 cm^{-1} frequency shift. The other contributions to the 10 nm Raman emission band come from two 10 nm wavebands, one above and one below the main source waveband. Water Raman scattering coefficients appropriate to the frequency shift from the upper and lower source wavelengths are then applied to determine the contributions of these wavebands to the emission waveband being studied. A new feature incorporated into the NOARL optical model is the variations in the phase function for Raman scattering. The depolarization ratio varies across the Raman emission band. A high depolarization ratio, as found for the 3500 cm^{-1} frequency shift, yields a higher water Raman scattering coefficient with a phase function approaching the spherical in shape. A low depolarization ratio, as found for the 3150 cm^{-1} frequency shift, yields a lower water Raman scattering coefficient with a phase function approaching the classic "dumbbell" shape.[3] Each source wavelength feeding into the defined water Raman emission band therefore generated a different phase function at the emission band depending on the average depolarization ratio for that Raman emission band. The phase functions were determined with the relations reported by Marshall[3] and Schrötter and Klöckner.[25] This attention to what is happening in narrowly defined wavebands allows an accurate assessment of the generation of water Raman emission from a spectrally varying solar source interacting with

a marine hydrosol of spectrally varying optical properties.

The simulations were performed at 430 nm, 440 nm, 470 nm, 490 nm, 520 nm, 550 nm, 589 nm, 620 nm, 640 nm, and 660 nm. These wavelengths were chosen to span most of the regions of greatest optical activity, etc. of the marine hydrosol and to correspond with wavelengths actively being studied by many groups, including NOARL. At greater wavelengths we encounter the regions known to be strongly affected by chlorophyll fluorescence.

For a simulation run photons are transported through a clear atmosphere containing a marine aerosol for both a Raman emission wavelength and three Raman source wavelengths. The determination of the Raman source wavelengths for the emission wavelength is made on the basis of the frequency shifts discussed previously. The relative numbers of photons propagated at the three source wavebands and the one emission waveband are determined from the extraterrestrial solar irradiance spectrum reported by Iqbal.[26] The atmospheric model of Iqbal is then used to propagate solar and skylight photons through the marine aerosol to sea level. The angle of entry of a skylight photon is determined from the skylight radiance distribution of Harrison and Coombes,[27] while the entry angle of a solar photon is at 11° from the zenith. The sea surface is flat. At the air/water interface the photon will either enter the ocean and be refracted or will be reflected back into the air based on the laws of Fresnel and Snell. These laws

determine the probabilities of these events that are chosen by a random number generator. Upon entry into the ocean a photon can be absorbed, scattered, or transpectrally scattered. The probabilities of these events are determined from the respective coefficients of the model, the individual events are chosen by a random number generator. The absorption of a photon automatically generates a new one that propagates through the system until 2.5×10^6 photons have been propagated. Counters set up at regular depth intervals sum up the photons passing through that interval and thus their sums are directly proportional to radiances and irradiances as they would be measured by a photometer. Duplicate runs are made for the wavelength studied.

IV. Results

First we will examine the results from the portion of the simulated irradiance field which is most sensitive to the effects of water Raman scattering: the upwelling irradiance field, E_u. In Fig. 1 we have plotted the logarithm of the upwelling irradiance from the separate streams of solar photons and water Raman photons, and the combined stream as an irradiance meter would read them. The absolute number of upwelling Raman photons increases with a decrease in wavelength (Fig. 1a-j). The only

exception is at 440 nm (Fig. 1b) where the quantity of upwelling Raman photons is less than that at 470 nm (Fig. 1c). We also note that the apparent decay rate of water Raman photons with depth relative to that of the solar photons decreases with increase in wavelength. The solar photons exhibit the exponential decay of a photon source at the water surface. The change in water Raman photons with depth, however, is a complex balance between photon generation, decay, and diversion by multiple elastic scattering. The increase of the decay rate of solar photons relative to Raman photons with depth, with increase in wavelength, causes the water Raman photons to eventually dominate the upwelling irradiance. In the region 430 - 490 nm there is either a small Raman contribution to the total photons at the surface or a relatively small and constant contribution with depth (Fig. 1a-d). In the region 520 - 589 nm, the upwelling irradiance field is composed of 50% Raman photons at depths ranging from 50 m to 20 m with increase in wavelength (Fig. 1e-g). In the region 620 - 660 nm, the upwelling irradiance field is composed of 50% Raman photons at depths ranging from 10 m to 5 m with increase of wavelength (Fig. 1h-j).

The contribution of Raman photons to the total photic field is also significant. Consider the percentile of the scalar irradiance, E_o, that is contributed by Raman photons across the spectrum. Table 1. indicates the percentile contribution of

Raman photons in the surface layer, which is a good index of the total water Raman scattering activity for a given wavelength. In the surface layer we are receiving the transpectrally scattered photons from the maximum possible source at the surface plus the water Raman photons integrated from all depths below the surface. The maximum contribution from water Raman scattering comes at 430 nm where it amounts to 1.7% of the scalar irradiance. The percentile contribution drops steadily with wavelength to 660 nm where it amounts to 0.043% of the scalar irradiance. The only exception is at 440 nm where the percentile contribution from water Raman scattering is less than at 470 nm. The percentile contribution of water Raman photons to the scalar irradiance with depth and wavelength is in Fig. 2. The method used here is the calculation of the absorption coefficient anomaly, applicable to field data, as proposed by Stavn and Weidemann[2]

$$\frac{\Delta a(z)}{a(z)} \cong \frac{E_o^*(z)}{\left[E_o(z) + E_o^*(z)\right]} , \qquad (1)$$

where $\Delta a(z)/a(z)$ is the absorption coefficient anomaly at depth z, $E_o^*(z)$ is the scalar irradiance due to water Raman photons at that depth, and $E_o(z)$ is the scalar irradiance due to solar photons at that depth. The numerator of the absorption coefficient anomaly is simply the difference between the absorption coefficient calculated from a non-conservative photic field and the actual absorption coefficient as measured in a

spectrophotometer. The non-conservative absorption coefficient is calculated from the non-conservative irradiance field by Gershun's equation,[2]

$$\tilde{a}(z) = - \frac{1}{\left[E_o(z) + E_o^*(z)\right]} \times \frac{d\left[E_z(z) + E_z^*(z)\right]}{dz}, \qquad (2)$$

where $E_z = E_d - E_u$ is the net downwelling irradiance or downwelling vector irradiance for solar photons, $E_z^*(z)$ is the net downwelling irradiance from water Raman photons, and $\tilde{a}(z)$ is the non-conservative absorption coefficient. In the region of 430 - 470 nm the contribution of water Raman scattering to the total photic field is nearly inconsequential (Fig. 2a-c). At 490 nm there is a small and nearly constant contribution of water Raman photons with depth (Fig. 2d). At 520 nm and 550 nm the Raman contribution is 50% at 140 m and 100 m respectively (Fig. 2e,f). For 589 nm we have a transition region where the Raman contribution becomes more important at lesser and lesser depths (Fig. 2g). At this wavelength the scalar irradiance field is composed of 50% Raman photons at 60 m. In the region 620 nm to 660 nm the depth of the 50% contribution of Raman photons to the scalar irradiance decreases from 30 m to 20 m (Fig. 2h-j).

The light field property in these simulations of greatest

interest to remote sensing and many light field parameterizations is the irradiance ratio R, the ratio of the upwelling irradiance to the downwelling irradiance, E_u/E_d. In Fig. 3 are plotted the R values for the backscattered portion of the directly transmitted solar photons and also the R value for the total photons, solar plus Raman. At 430 nm and 440 nm the R value is significantly affected by water Raman photons only in the surface layers; the effect decreases with depth to inconsequential levels (Fig. 3a,b). At 470 nm and 490 nm the Raman contribution to the total photons becomes noticeable at greater depths (Fig. 3c,d). In this general region of blue to blue-green, the R value for total photons appears to be nearly constant with depth, while the R value for solar photons alone tends to increase with depth. In the region 520 nm to 589 nm the R value shows a tendency to increase way beyond the accepted values for R in a conservative system with small backscattering coefficients (Fig. 3e-g). In the region 620nm - 660 nm the dramatic increase in R occurs at shallower and shallower depths (Fig.3h-j). In general, the effects of water Raman scattering on R are significant only in the surface layers at wavelengths below 470 nm while the effects become dramatic with depth for wavelengths greater than 470 nm. There is also a slight decrease in R for total upwelling photons at 440 nm (Fig. 3b).

To illuminate the possibilities for the effects of water

Raman scattering on the remotely detected (by satellite or aircraft) upwelling irradiance in air, the R values in air are plotted in Fig. 4. At 430 nm the Raman contribution to the R value in air is 6% with about a 1% drop in Raman contribution at 440 nm. The Raman contribution steadily increases to 550 nm where it is about 15% of the total R value. Beyond 550 nm the Raman contribution to the R value drops slightly and holds more-or-less steadily to 660 nm where it is about 13% of the R value.

V. The Clear Ocean Radiant Flux Field: Raman Contributions across the Spectrum

Consider now the mechanisms behind the observations from the Monte Carlo output and the implications of these observations for future work and algorithms relating ocean optics to variations in chlorophyll concentration, predictions of primary productivity, etc.

We have amassed considerable evidence for the contribution of water Raman scattering to the photic field of clear ocean waters. For example, the percentile contributions of water Raman photons in the surface layer are documented in Table 1. The greatest absolute contribution of water Raman photons is at 430 nm (1.7% of the photic field) and the absolute contribution decreases with an increase in wavelength. Given the nearly

constant or at least comparable numbers of solar photons across the spectrum that are present in the surface layers,[28] and the λ^{-4} relation for the generation of water Raman photons, this result is not surprising. However, the trend in the percentage of water Raman photons at the surface does not follow this power law but has a smaller slope instead. This result indicates that multiple elastic scattering and multiple interreflections off the interface are concentrating the water Raman photons in the process called optical energy trapping.[29,30] In addition, there is a slight drop in the percentage of water Raman photons at 440 nm which can be explained as a result of Fraunhofer line effects in the insolation. The major source of Raman photons emitted at 440 nm is the solar photons in the wavelength region of about 375 nm to 395 nm. There are significant decreases in the flux of solar photons in this region due to strong Fraunhofer lines: the L line for Fe centered at 383 nm, and the K line for Ca centered at 393 nm. This Fraunhofer line effect shows up elsewhere.

Obviously, the significance of the effect of water Raman photons on the irradiances, etc. of the submarine light field is not just a function of the absolute production of Raman photons. Also we have to consider that the absorption coefficient of the marine hydrosol varies spectrally: at longer wavelengths the absorption is relatively high and due essentially to the water molecule. That is, we cannot consider just the production of

water Raman photons but also their differential removal relative to the more-or-less overwhelming stream of solar photons. The water Raman scattering coefficient is approximately one tenth the magnitude of the scattering coefficient of the water molecule[4] and thus has the potential to contribute photons to the field at the emission wavelength. However, if the hydrosol absorption coefficient is relatively large at the emission wavelength and a significant amount of solar photons is removed, the potential contribution of water Raman photons to the photic field at the emission wavelength could be considerable. Assuming again that the number of photons from insolation is comparable across most of the visible spectrum, we can analyze a simple ratio of the absorption coefficients for the hydrosol to predict the probable significance of water Raman scattering. In Table 2. are listed, at the Raman emission wavelengths, the ratio of the hydrosol absorption coefficient at the Raman emission wavelength to the hydrosol absorption coefficient at the source wavelength. The absorption coefficient at the source wavelength is a weighted average of the absorption coefficients of the hydrosol at the three wavebands contributing Raman photons to the emission waveband. The weighting function for the three source absorption coefficients is the Raman scattering coefficient operating at that source waveband to produce Raman photons at the given emission waveband. The hydrosol of the oligotrophic ocean has an

absorption coefficient that is due mostly to water. Thus the minimum of this absorption coefficient is at 430-450 nm with increases in the coefficient both toward the blue end and the red end of the spectrum.

Thus there are three general regions of Raman effects in the open ocean based on both the increase of hydrosol absorption toward blue-UV and red regions relative to blue, and the 55-100 nm wavelength shift for transpectrally scattered photons (see Table 2.). In the region of 380-460 nm the absorption coefficient at the Raman source wavelength is greater than the absorption coefficient at the Raman emission wavelength; this greatly reduces the effects of water Raman scattering. The absorption coefficient ratio of less than 1.0 in this region implies that the decay rate of the large flux of solar photons at the emission wavelength will be less than the net production rate of Raman photons. This large flux of solar photons at the emission wavelength will penetrate to great depths, while potential source photons for Raman scattering will decay at a greater rate and not penetrate very deeply. The net production of Raman photons will be less and less with depth. Thus the Raman photons will be at a decreasing percentage of the total light field with depth and will have their strongest effect, if any, in the surface layers. In the region of 470-490 nm the hydrosol absorption coefficient at the Raman source wavelength is

approximately equal to the absorption coefficient at the Raman emission wavelength and the production of Raman photons should make a nearly constant, and small, proportion of the light field with depth at the emission wavelength. In the region of 490-660 nm the absorption coefficient at the source wavelength for Raman scattering is less than the absorption coefficient at the emission wavelength. This implies that the decay rate of the solar photons at the emission wavelength for Raman scattering will be much greater than the net production rate of Raman photons, since there will be a relatively large flux of potential source photons with depth. In this case we expect that the in-water effects of Raman scattering will be a dominant influence with depth as the solar photons are strongly removed and only Raman photons are left behind. This trend should continue throughout the longer wavelengths of the visible spectrum.

What are the effects, then, of water Raman scattering with depth relative to the predictions above? From Fig. 2 we see that at wavelengths less than 470 nm, approaching the blue/violet end of the visible spectrum, the penetrating solar photons at the Raman source wavelengths are removed more rapidly than solar photons at the emission wavelengths because the Raman emission effects are masked by the relatively large amount of solar photons with depth at the emission wavelength. At 470 - 490 nm we have a transition region where the Raman emission has a small

but steady effect as the light field penetrates the clear ocean hydrosol. The absorption of both potential Raman source photons and the solar photons at the emission wavelength are about equal. In the region greater than 500 nm wavelength the Raman contributions increase rapidly with depth. As we increase in wavelength the high hydrosol absorption at the emission wavelength rapidly removes solar photons and the remaining Raman photons dominate the field.

The water Raman photon contribution to the total light field makes the observations on the upwelling irradiances clear and explicable. Given the small backscattering coefficient in the marine hydrosol, it is reasonable that Raman emission can make a significant contribution to the upwelling irradiant flux. We see from Fig. 1 that the greatest absolute contribution to the upwelling irradiance from Raman scattering occurs at the blue end of the spectrum and decreases toward the red end, with a slight dip due to Fraunhofer line effects at 440 nm. The apparent decay rate of the Raman photons with depth at nearly all wavelengths appears to be constant. This apparent rate of decay is of course a complex rate involved with the production of Raman photons with depth interacting with the absorption coefficient of the hydrosol, etc. However, the decay rate of the solar upwelling photons with depth increases dramatically with wavelength as would be predicted from Table 2. Thus, the contribution of Raman

photons to the deep photic field increases with wavelength at greater than 500 nm even though the absolute production of Raman photons is dropping off. In the extreme red end the upwelling irradiance field is dominated by Raman photons very quickly at rather shallow depths. And in the blue/violet end of the spectrum the contribution of Raman photons drops off with depth as the decay rate of the potential Raman source photons in the blue/violet region increases compared to the relatively low decay rate of the solar photons at the emission wavelengths. Thus, the influence of the Raman photons on the upwelling irradiance field at the blue/violet end of the spectrum is confined to the surface layers.

Certainly the irradiance ratio is the light field parameter detectable by remote sensing through the upwelling irradiance and is thereby worthy of consideration. Many algorithms attempt an inversion of the irradiance ratio R to determine the spatial distribution and concentration of the components of the hydrosol. One empirical mode of inversion involves determining the irradiance ratios for different wavelengths and calculating the ratio of the different R values. Thus it is important to see if water Raman scattering will affect the R ratio. From Fig. 3 we see that the irradiance ratio of solar photons at the blue end of the spectrum increases steadily with depth, while the addition of water Raman photons primarily at the surface causes the in-water

irradiance ratio to be nearly constant with depth. At wavelengths greater than 500 nm the relatively fast disappearance of solar photons with depth causes the irradiance ratio to increase with depth to values beyond the usual maxima for a system dominated by elastic scattering. The irradiance ratios in air from Fig. 4 show an augmentation by Raman photons at 430 nm of about 6%; this augmentation increases to a maximum of about 15% at 550 nm. There is also a slight dip at 440 nm attributable to Fraunhofer line effects. Beyond 550 nm the augmentation is a little less and nearly constant out to 660 nm. From Table 2. we see that the ratio of absorption coefficients for the hydrosol increases steeply up to the region of 550 - 589 nm, then tends to level off. Between 500 nm and 600 nm the absorption coefficient at the Raman emission wavelength causes the rate of decay of the solar photons at that wavelength to increase faster than the drop off of Raman photon production from the λ^{-4} relationship. Thus the increase in the percentile composition of Raman photons in this region of the visible spectrum. Beyond 600 nm the decay rate of solar photons appears to balance the decrease in Raman photon production. The Raman photon production can also be augmented by multiple scattering and optical energy trapping of solar photons at the Raman source wavelength. The increase in the absorption coefficient with increase in wavelength is accompanied by a decrease in the scattering coefficient of the

hydrosol which implies less opportunity for multiple scattering effects to occur at the emission wavelength.

In summary two major trends are at work in clear ocean water. There is a greater production of Raman photons at the blue end of the visible spectrum and a greater absorption of solar photons at the red end of the visible spectrum — how do these trends "translate" into the typical optical events of the oligotrophic ocean? At the shortwave end of the spectrum the production of Raman photons affects the submarine light field primarily at the surface. As depth increases the production of Raman photons is masked by the relatively powerful solar photon stream at the Raman emission wavelength. As we approach the longwave end of the spectrum, Raman photons are produced in a region of relatively low marine hydrosol absorption which allows significant production of Raman photons for relatively great depths of penetration. The wavelength shift of the Raman photons places them at a wavelength where the hydrosol removes solar photons quickly and the solar photon stream diminishes rapidly with depth. Under these conditions, the light field can become dominated by Raman photons at greater and greater depths. This occurs even though the absolute production of Raman photons decreases with increase in wavelength. The backscatter of downward penetrating solar photons also diminishes with wavelength since it is primarily fluctuation theory

(Rayleigh-type) scattering. The increased absorption of solar photons also diminishes the magnitude of the backscattering process. Thus the upwelling irradiance in air has a significant Raman component which increases with wavelength. The balance between the decrease in solar photons, decrease in backscattering, and lesser decrease in Raman photon production causes the Raman component to increase in its contribution to the irradiance ratio R until it peaks at 550 nm. These processes tend to be in balance to the extreme wavelength of this study, 660 nm, and the Raman contribution to R remains constant in this region.

These results have many important implications. It has often been reported that the in-water irradiance ratio R is constant for the wavelength region of 430 - 490 nm. It is evident here that this apparent constancy of R is probably an artifact resulting from water Raman scattering effects at the surface. Multiple scattering of solar photons clearly dictates an increase in R with depth and the augmentation of the upwelling irradiance by water Raman scattering at the surface creates this apparent constancy. Many remote sensing algorithms rely on ratios of R at various key wavelengths for inverting concentrations of chlorophyll, etc. from these ratios. The contribution of water Raman scattering to the value of R in air will be variable depending on the absorption spectrum of these

materials, and it is also variable itself across the visible spectrum, peaking at 550 nm. Additionally, the Raman contribution at 440 nm is reduced because the photon flux at the source wavelengths is reduced due to the presence of Fraunhofer L and K lines at the source wavelengths. This spectral variation of the Raman contribution to R renders suspect the various ratioing schemes for remote sensing using R. The corruption of the upwelling signal by Raman scattering will dictate continual "calibration" of these algorithms with "sea-truth" data and restriction of certain algorithms to specific regions of the ocean until processes like Raman scattering are properly factored in. Thus far we have delineated major factors to consider in the effects of water Raman scattering on the optical properties of the oligotrophic ocean. Much remains to be done. The indications that optical energy trapping off the water/air interface may be of significance in concentrating Raman photons require simulations with a wave-disturbed interface. The interactions of skylight and solar zenith are also required. The possibility of water Raman "windows" in the water types up through the green coastal waters also remain to be explored.

This paper is produced as part of the Optical Oceanography Program, formerly NOARL and now Naval Research Laboratories

Detachment, directed by Rudolph Hollman. At UNCG I received the support of the Statistical Consulting Center and Computing and Information Systems. For the numerous insights derived from discussions with Alan Weidemann, Rudolph Hollman, Kendall Carder, Frank Hoge, and Ken Ferer I am thankful. I am pleased to acknowledge the continuing support of the Office of Naval Research, Grant No. N00014-89-J-3137/P00002

References

1. R. H. Stavn and A. D. Weidemann, "Optical Modeling of Clear Ocean Light Fields: Raman Scattering Effects," Appl. Opt. 27, 4002-4010 (1988).
2. R. H. Stavn and A. D. Weidemann. 1992. Raman scattering in ocean optics: quantitative assessment of internal radiant emission. Appl. Opt., 31:1294-1303.
3. B. R. Marshall, "Raman scattering in ocean water," Master's Thesis, Geography Department, U. California at Santa Barbara (1989).
4. B. R. Marshall and R. C. Smith, "Raman scattering and in-water optical properties", Appl. Opt. 29, 71-84 (1990).
5. S. Sugihara, M. Kishino, and M. Okami, "Contribution of Raman Scattering to Upward Irradiance in the sea", J. Oceanogr. Soc. Japan, 397-404 (1984).

6. D. A. Long, Raman Spectroscopy. (McGraw-Hill, New York, 1977), 276 p.

7. R. C. Smith and K. S. Baker, "Stratospheric ozone, middle ultraviolet radiation and phytoplankton productivity", Oceanography, 4-10 (1989).

8. H. R. Gordon, "Diffuse reflectance of the Ocean: Influence of nonuniform phytoplankton pigment profile," Appl. Opt. 31, 2116-2129 (1992).

9. H. R. Gordon and A. Y. Morel, Remote Assessment of Ocean Color for Interpretation of Satellite Visible Imagery: A Review (Springer-Verlag, New York, 1983), 114 p.

10. H. R. Gordon, "Diffuse Reflectance of the Ocean: the Theory of its Augmentation by Chlorophyll a Fluorescence at 685 nm," Appl. Opt. 18, 1161-1166 (1979).

11. C. H. Mazel, "Spectral Transformation of Downwelling Radiation by Autofluorescent Organisms in the Sea," Proc. Soc. Photo-Opt. Instrum. Eng. 1302-Ocean Optics X, 320-327 (1990).

12. E. D. Traganza, "Fluorescence Excitation and Emission Spectra of Dissolved Organic Matter in Sea Water," Bull. Mar. Sci. 19, 897-904 (1969).

13. K. Carder, R. G. Steward, G. R. Harvey, and P. B. Ortner, "Marine Humic and Fulvic Acids: Their Effects on Remote Sensing of Ocean Chlorophyll," Limnol. Oceanogr. 34, 68-81

(1989).

14. F. E. Hoge and R. N. Swift, "Delineation of estuarine fronts in the German Bight using airborne laser-induced water Raman backscatter and fluorescence of water column constituents," Int. J. Remote Sensing 3, 475-495 (1982).

15. G. N. Plass and G. W. Kattawar, "Monte Carlo Calculations of Radiative Transfer in the Earth's Atmosphere-Ocean System: 1. Flux in the Atmosphere and Ocean," J. Phys. Oceanogr. 2, 139-145 (1972).

16. H. R. Gordon and O. B. Brown, "Irradiance Reflectivity of a Flat Ocean as a Function of its Optical Properties," Appl. Opt. 12, 1549-1551 (1973).

17. J. T. O. Kirk, "Monte Carlo Procedure for Simulating the Penetration of Light into Natural Waters," CSIRO Div. Plant Ind. Technol. Pap. 36, 36 pp. (1981).

18. R. C. Smith and K. S. Baker, "Optical Properties of the Clearest Natural Waters (200-800 nm)," Appl. Opt. 20, 177-184 (1981).

19. A. C. Tam and C. K. N. Patel, "Optical Absorption of Light and Heavy Water by Laser Optoacoustic Spectroscopy," Appl. Opt. 18, 3348-3358 (1979).

20. T. G. Peacock, K. L. Carder, C. O. Davis and R. G. Steward, "Effects of Fluorescence and Water Raman Scattering on Models of Remote Sensing Reflectance," Proc. Soc. Photo-Opt.

Instrum. Eng. 1302-Ocean Optics X, 303-319 (1990).

21. A. Morel, "Optical Properties of Pure Water and Pure Sea Water," in Optical Aspects of Oceanography, N. G. Jerlov and E. S. Steemann Nielsen, Eds. (Academic Press, London 1974).

22. G. Kullenberg, "Scattering of Light by Sargasso Sea Water," Deep-Sea Res. 15, 423-432 (1968).

23. T. J. Petzold, "Volume scattering functions for selected ocean waters", Univ. California, San Diego, Scripps Inst. of Oceanography, San Diego, CA, SIO Ref. 72-78 (October 1972).

24. W. F. Murphy and H. J. Bernstein, "Raman spectra and an assignment of the vibrational stretching region of water". J. Phys. Chem. 76, 1147-1152 (1972).

25. H.W. Schrötter and H.W. Klöckner, "Raman scattering cross sections in gases and liquids," in Raman Scattering of Gases and Liquids, A. Weber Ed. (Springer-Verlag, Series: Topics in Current Physics 11, Berlin, 1979) p. 123-166.

26. M. Iqbal, Solar Radiation (Academic, New York, 1984).

27. A. W. Harrison and C. A. Coombes, "Angular Distribution of Clear Sky Short Wavelength Radiance," Solar Energy 40, 57-63 (1988).

28. D. A. Siegel and T. D. Dickey, "On the Parameterization of Irradiance for Open Ocean Photoprocesses," J. Geophys. Res. 92, 14,648-14,662 (1987b).

29. R. H. Stavn, F. R. Schiebe, and C. L. Gallegos, "Optical controls on the radiant energy dynamics of the air/water interface: the average cosine and the absorption coefficient," Proc. Soc. Photo-Opt. Instrum. Eng. 489-Ocean Optics VII, 62-67 (1984).

30. R. H. Stavn, "The Three-Parameter Model of the Submarine Light Field: Radiant Energy Absorption and Trapping in Nepheloid Layers Recalculated," J. Geophys. Res. 92, 1934-1936 (1987).

Table 1.

Percentile Raman Contribution to Scalar Irradiance: Surface layer

Emission Wavelength:	430	440	470	490	520	550	589
	1.7084	**1.0991**	**1.2247**	**1.0767**	**0.5471**	**0.3765**	**0.1890**

Emission Wavelength:	620	640	660
	0.0757	**0.0661**	**0.0437**

Table 2.

Absorption Coefficient Ratio*

Emission Wavelength: (nm)	430	440		470	490	
	0.5437	**0.6619**		**0.9322**	**1.2829**	
Emission Wavelength: (nm)	520	550	589	620	640	660
	3.2860	**4.1041**	**6.0579**	**7.6966**	**6.4383**	**6.7544**

* $\left(\frac{\text{Absorption Coefficient (Emission } \lambda)}{\text{Weighted Absorption Coefficient (Source } \lambda s)} \right)$

Figure Captions

Fig. 1. Upwelling irradiances for solar photons, water Raman photons, and the combined total photons of clear ocean light field for a)430 nm, b)440 nm, c)470 nm, d)490 nm, e)520 nm f)550 nm, g)589 nm, h)620 nm, i)640 nm, j)660 nm. Standard error of the mean indicated by horizontal lines or thickness of line.

Fig. 2. Percentile contribution of water Raman photons to total light field (scalar irradiance) in clear ocean water with depth at a)430 nm, b)440 nm, c)470 nm, d)490 nm, e)520 nm f)550 nm, g)589 nm, h)620 nm, i)640 nm, j)660 nm. Note that the percentile scale goes to a maximum of 10% for graphs a) - d) and a maximum of 100% for graphs e) - j). The smaller percentile is necessary for the shorter wavelengths/fr to make their Raman contributions discernible.

Fig. 3. Irradiance ratios of clear ocean light field with depth for solar photons alone and total (solar + Raman) photons at a)430 nm, b)440 nm, c)470 nm, d)490 nm, e)520 nm, f)550 nm, g)589 nm, h)620 nm, i)640 nm, j)660 nm. Note that the R value has a maximum of 0.1 for graphs a) - d), 0.8 for graphs e) - g), and 1.0 for graphs h) - j).

Fig. 4. Irradiance ratios in air from clear ocean water with a flat surface for solar photons alone ( ), and total (solar + Raman) photons (——).

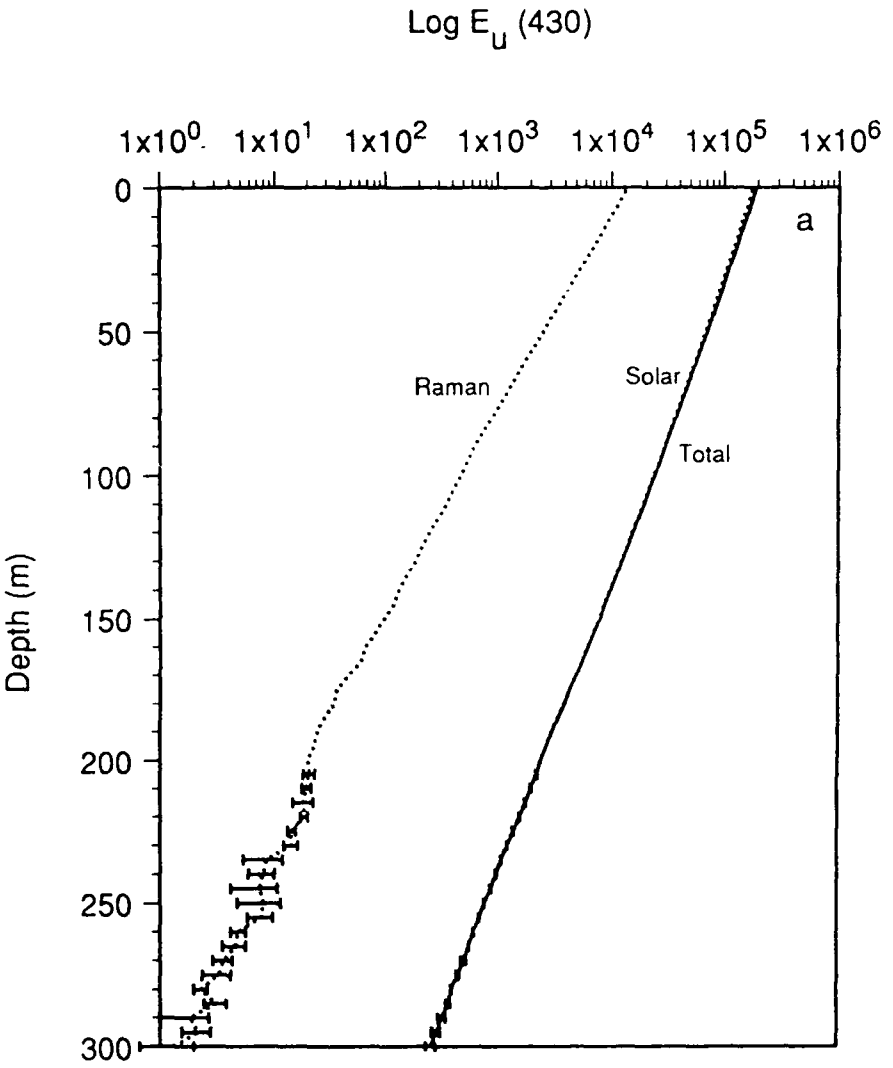
Log E_u (430)
1x10^0
1x10^1
1x10^2
1x10^3
1x10^4
1x10^5
1x10^6
0
50
100
150
200
250
300
Depth (m)
Raman
Solar
Total
a

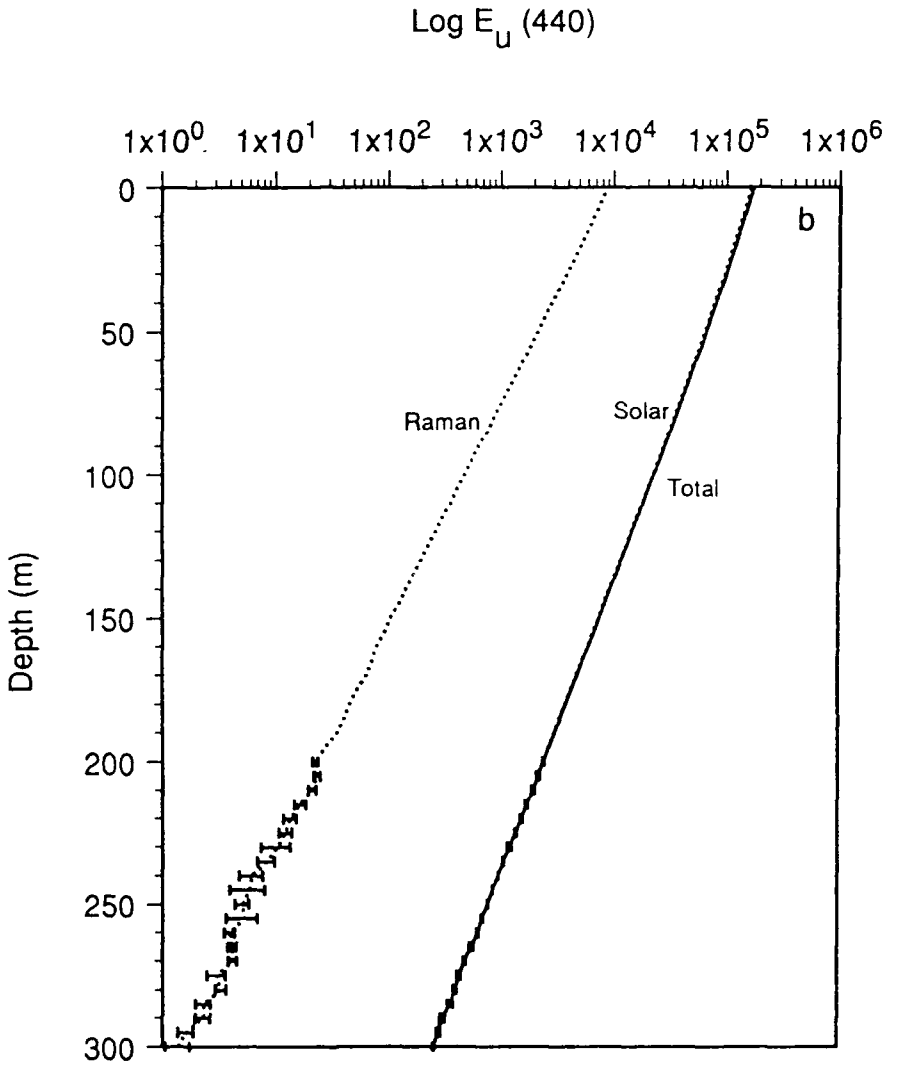
Log E_u (440)
1x10^0
1x10^1
1x10^2
1x10^3
1x10^4
1x10^5
1x10^6
0
50
100
150
200
250
300
Depth (m)
Raman
Solar
Total
b

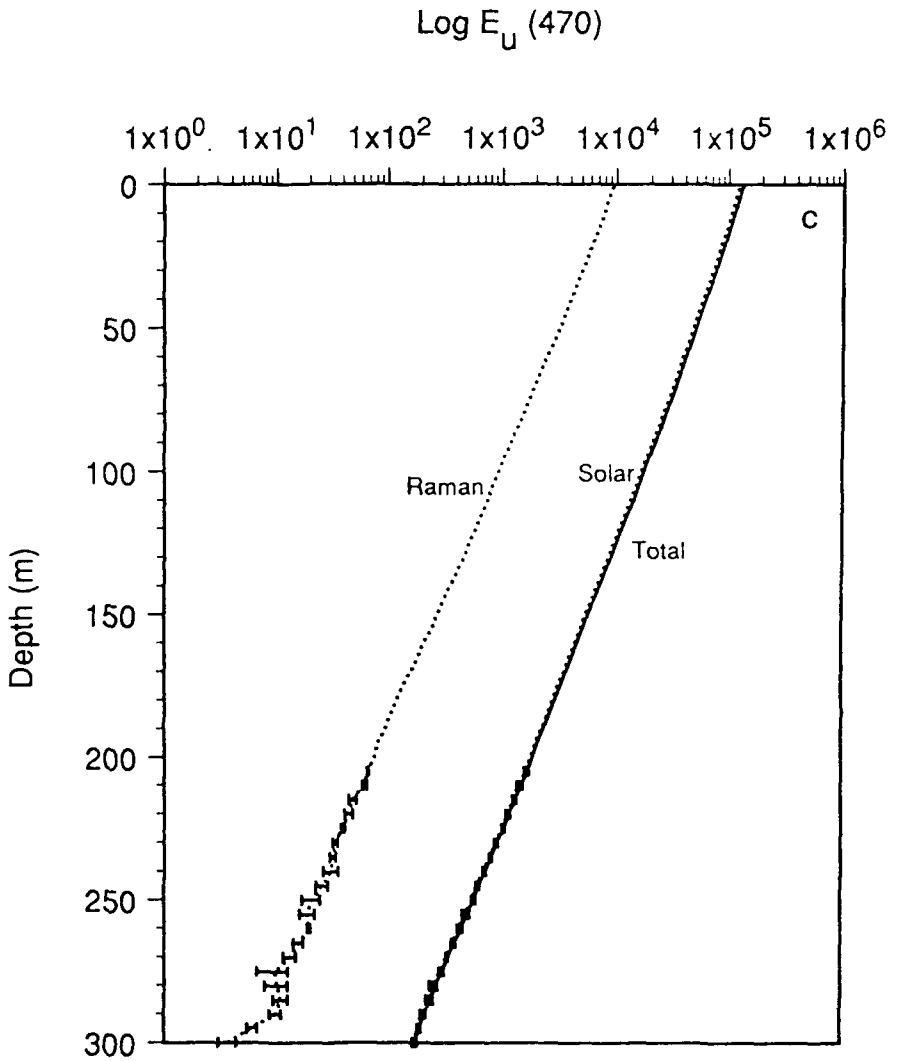
Log E_u (470)
1x10^0
1x10^1
1x10^2
1x10^3
1x10^4
1x10^5
1x10^6
0
50
100
150
200
250
300
Depth (m)
Raman
Solar
Total
c

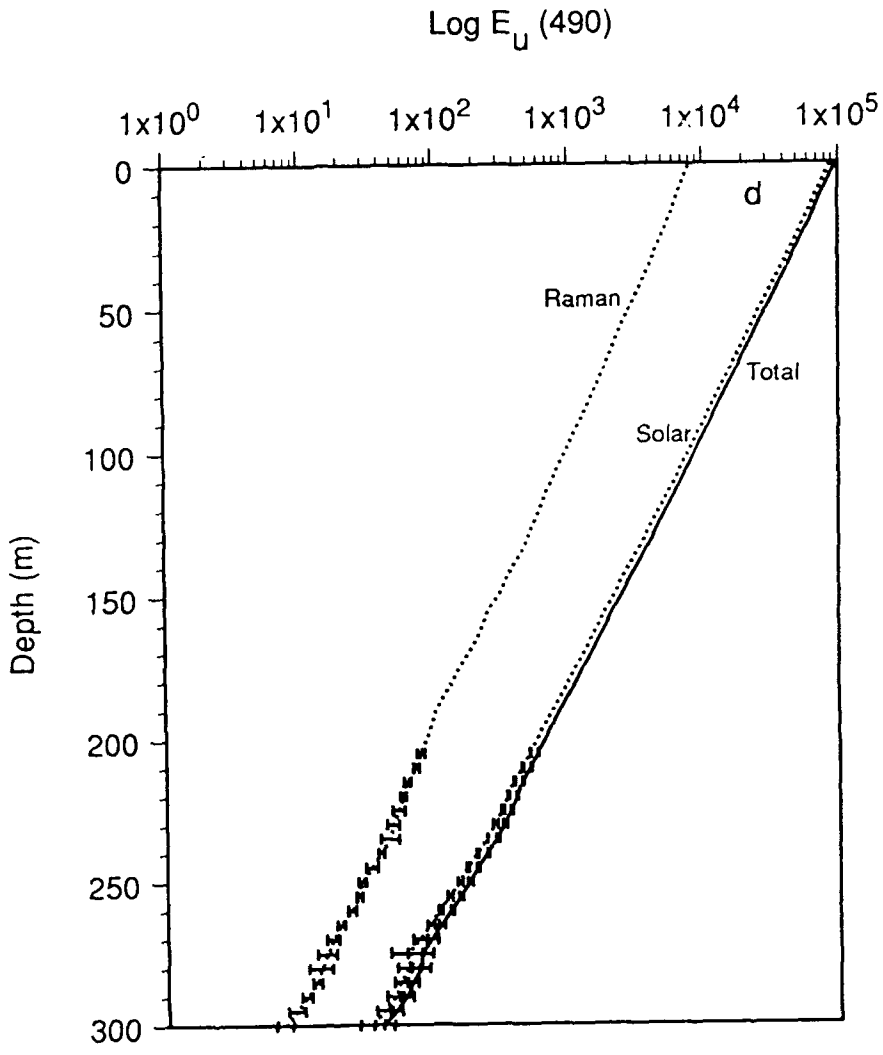
Log E_u (490)
1x10^0
1x10^1
1x10^2
1x10^3
1x10^4
1x10^5
0
50
100
150
200
250
300
Depth (m)
d
Raman
Total
Solar

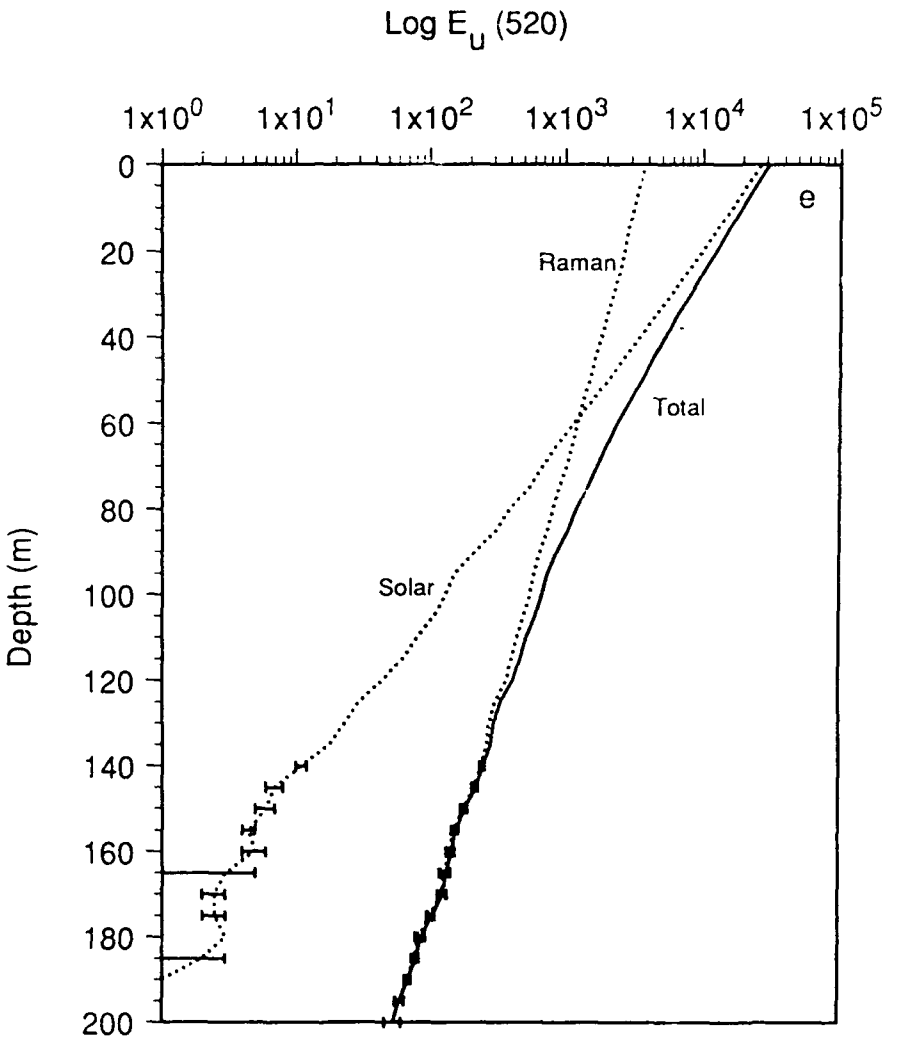
Log E_u (520)
1x10^0
1x10^1
1x10^2
1x10^3
1x10^4
1x10^5
0
20
40
60
80
100
120
140
160
180
200
Depth (m)
Raman
Total
Solar
e

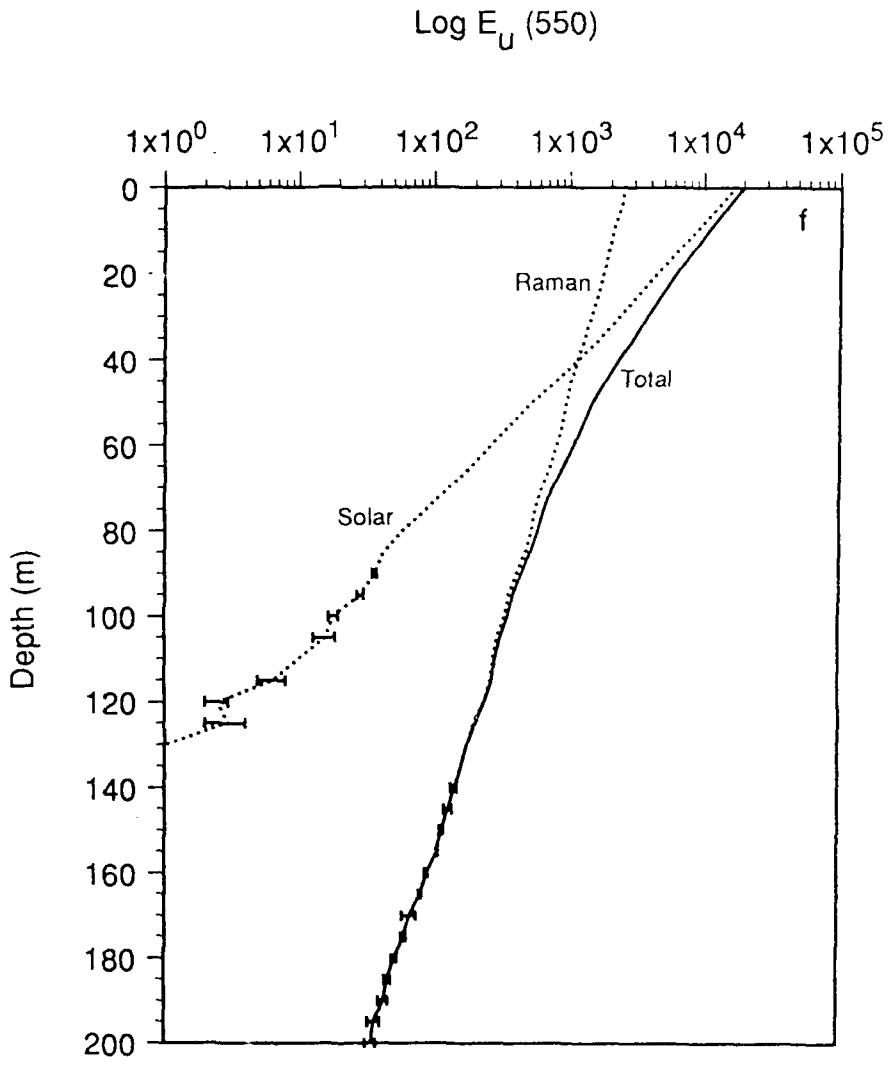
Log E_u (550)
1x10^0
1x10^1
1x10^2
1x10^3
1x10^4
1x10^5
0
20
40
60
80
100
120
140
160
180
200
Depth (m)
Raman
Total
Solar
f

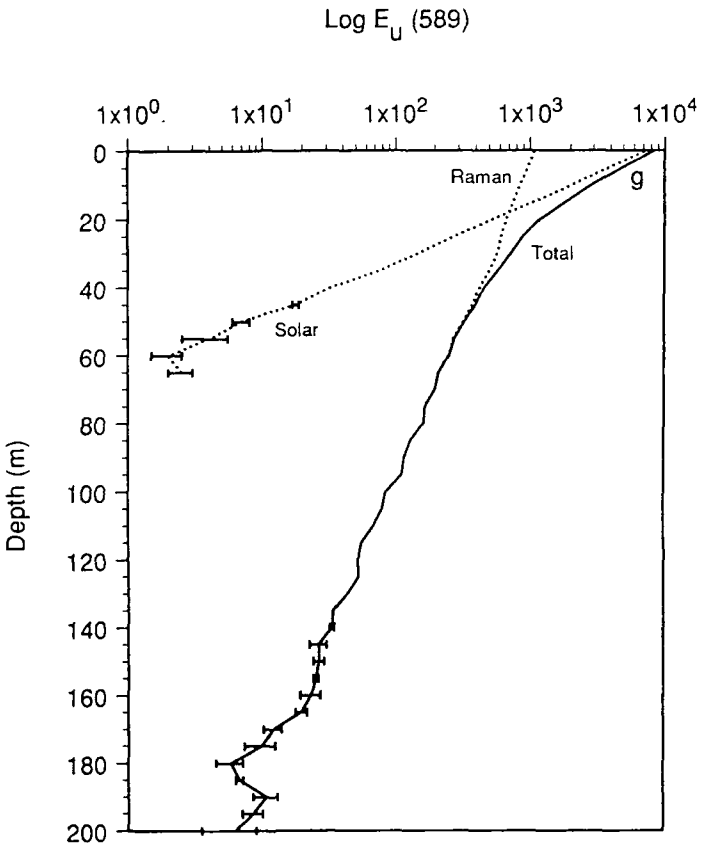
Log E_u (589)
1x10^0
1x10^1
1x10^2
1x10^3
1x10^4
0
20
40
60
80
100
120
140
160
180
200
Depth (m)
Raman
g
Total
Solar

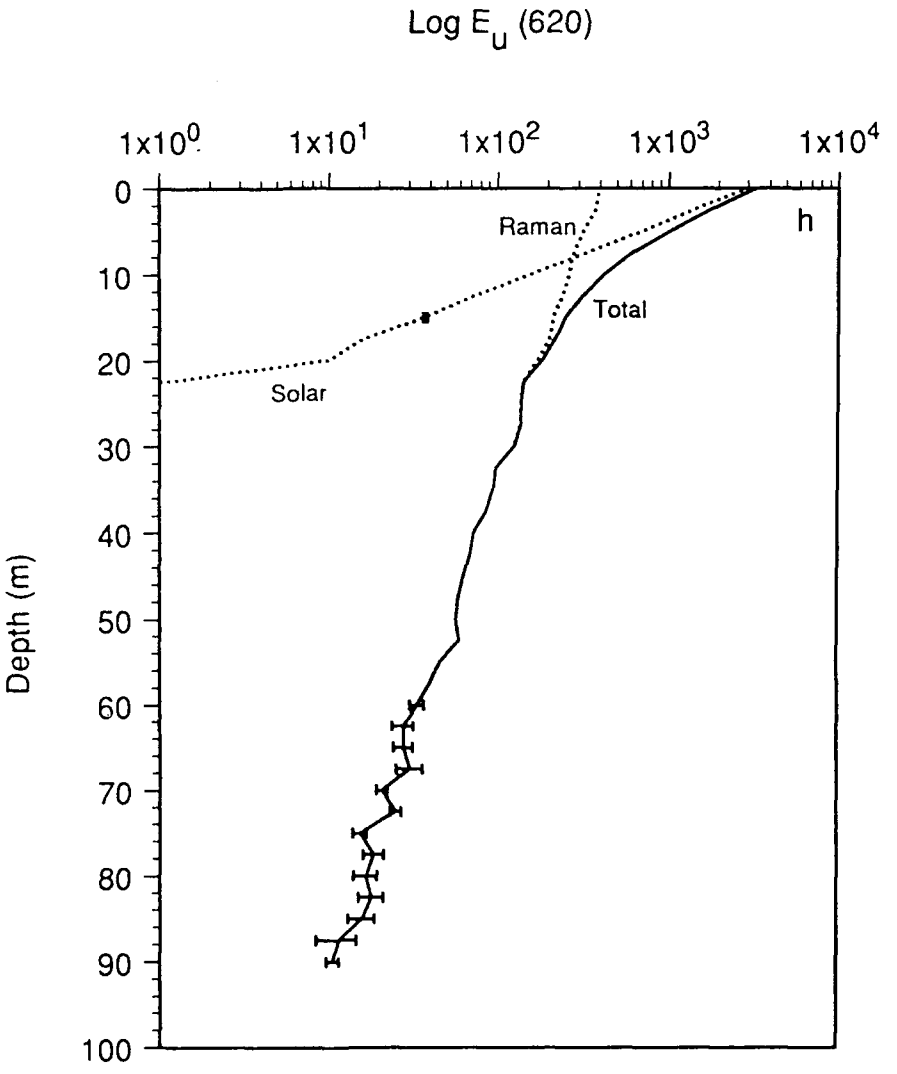
Log E_u (620)
1x10^0
1x10^1
1x10^2
1x10^3
1x10^4
0
10
20
30
40
50
60
70
80
90
100
Depth (m)
Raman
Total
Solar
h

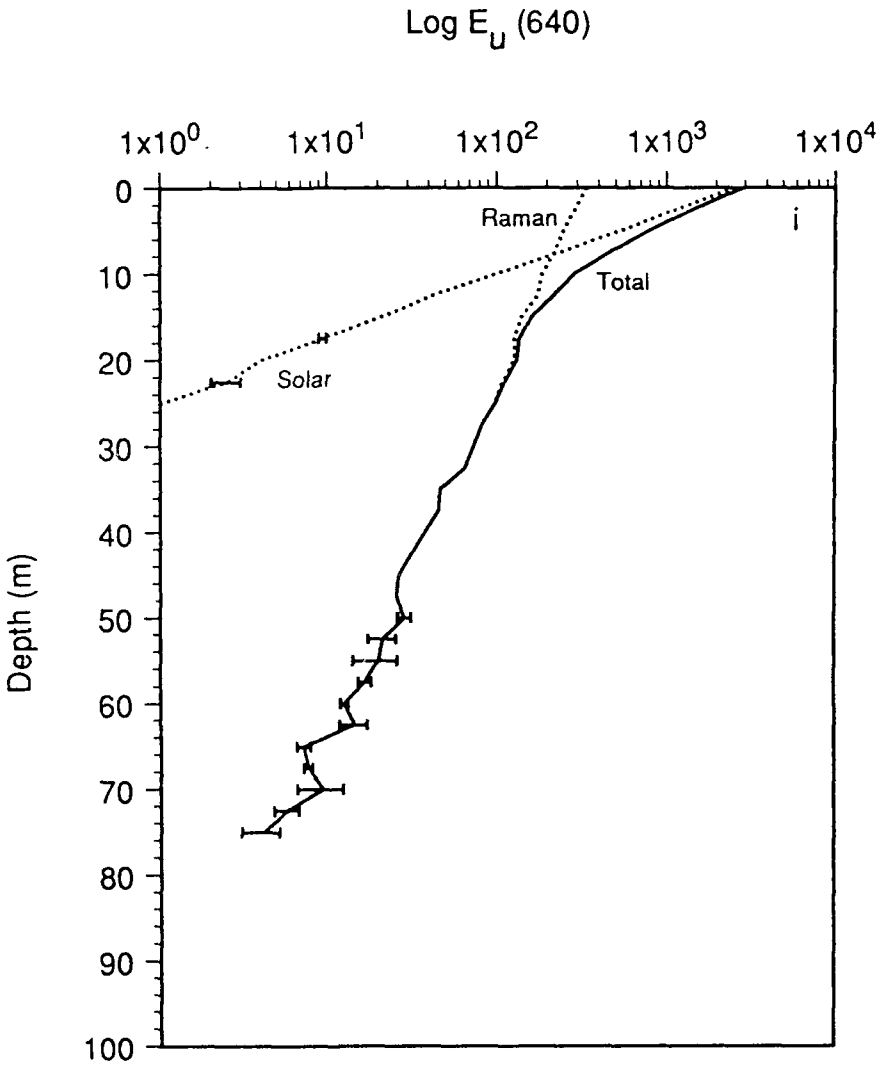
Log E_u (640)
1x10^0
1x10^1
1x10^2
1x10^3
1x10^4
0
10
20
30
40
50
60
70
80
90
100
Depth (m)
Raman
Total
Solar
i

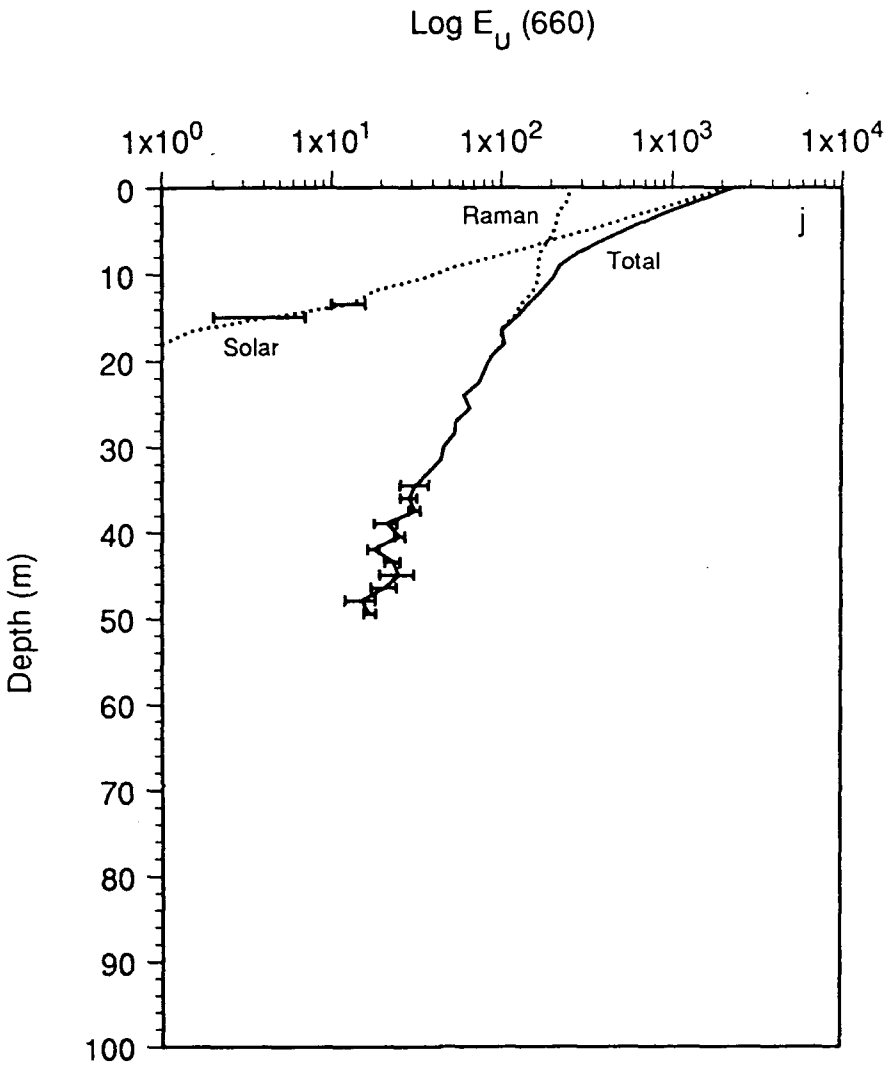
Log E_U (660)
1x10^0
1x10^1
1x10^2
1x10^3
1x10^4
0
10
20
30
40
50
60
70
80
90
100
Depth (m)
Raman
Total
Solar
j

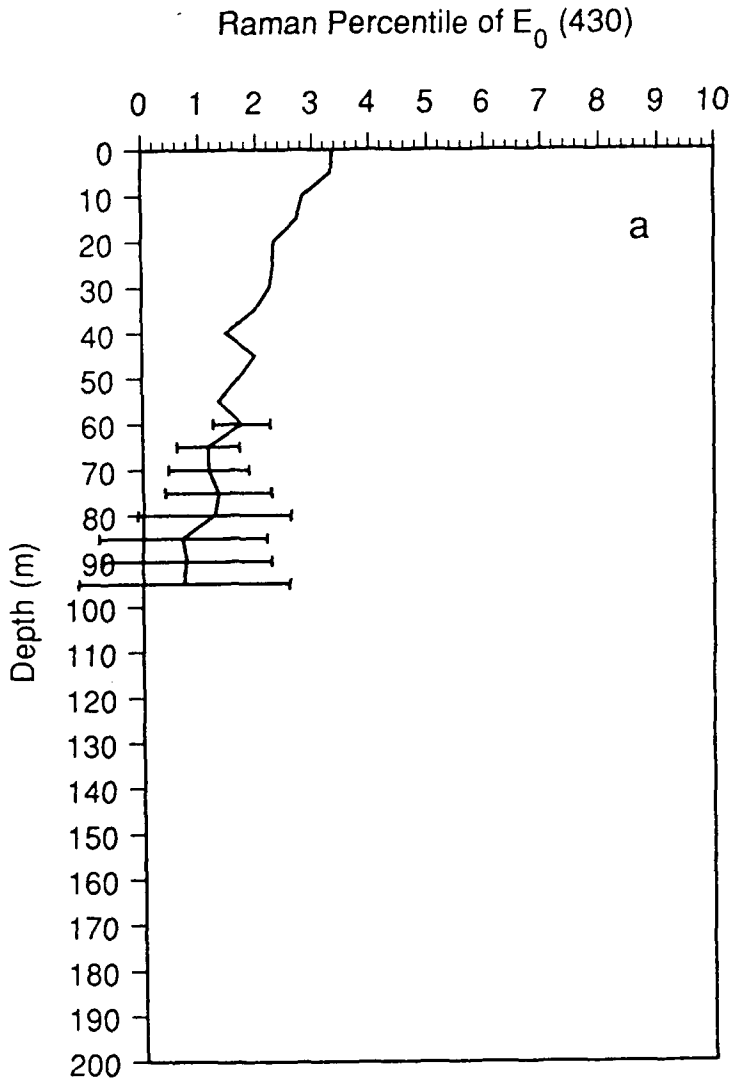
Raman Percentile of E_0 (430)
0 1 2 3 4 5 6 7 8 9 10
Depth (m)
0 10 20 30 40 50 60 70 80 90 100 110 120 130 140 150 160 170 180 190 200
a

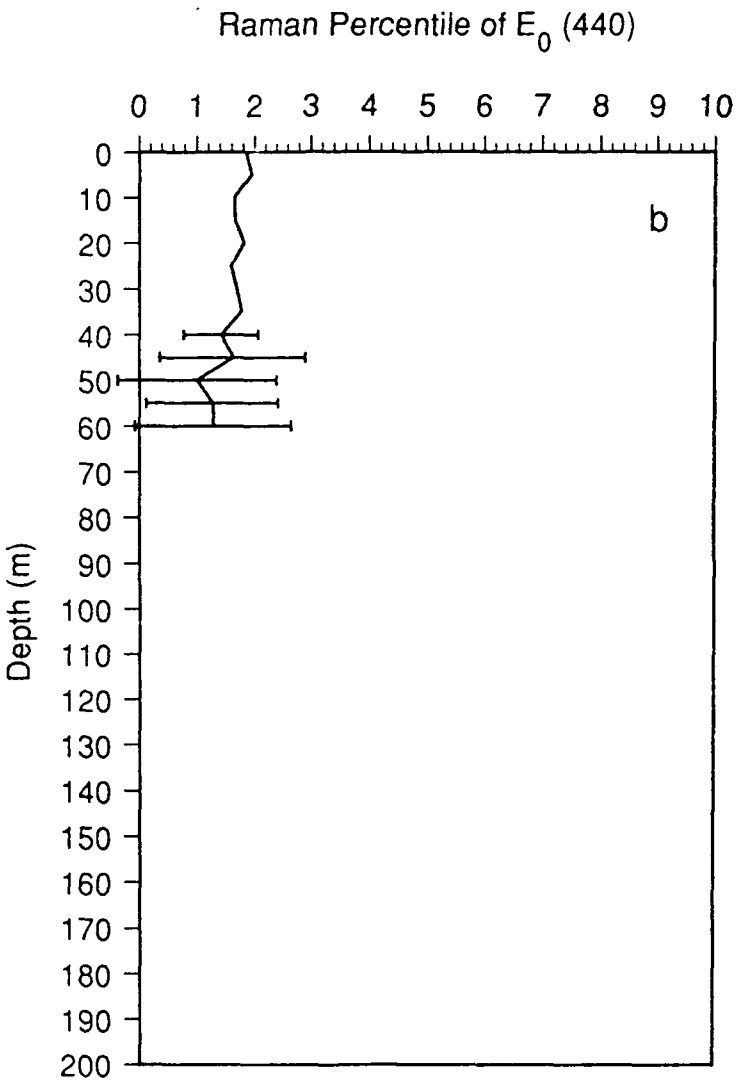
Raman Percentile of E_0 (440)
0 1 2 3 4 5 6 7 8 9 10
Depth (m)
0 10 20 30 40 50 60 70 80 90 100 110 120 130 140 150 160 170 180 190 200
b

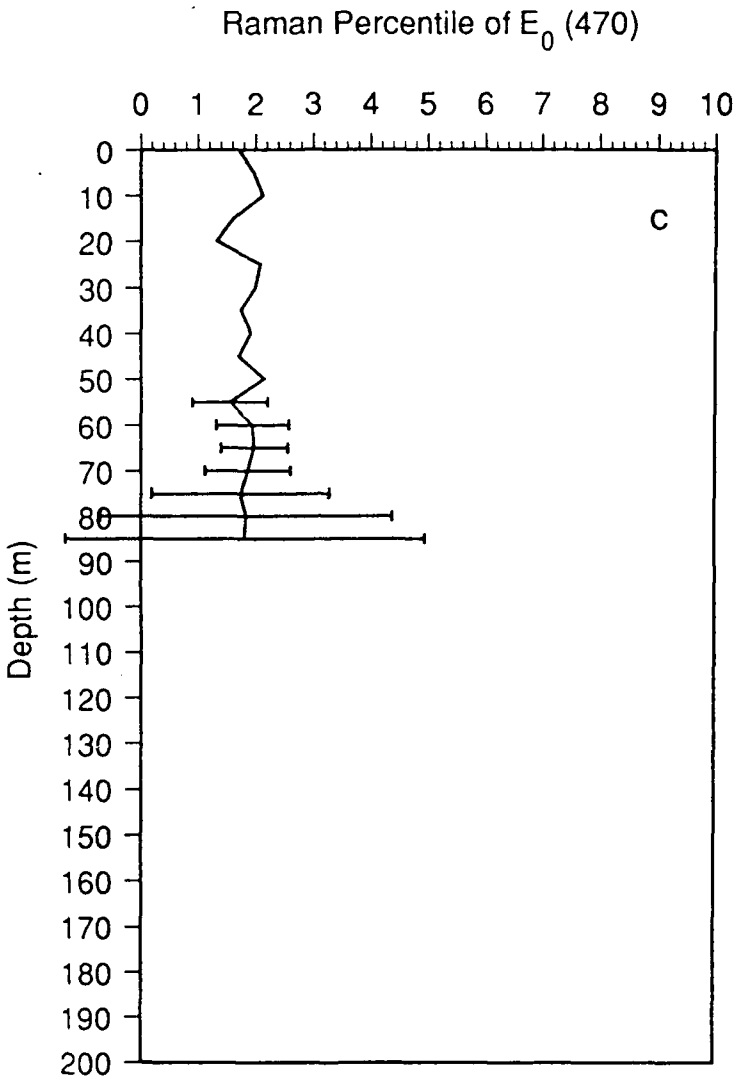
Raman Percentile of E_0 (470)
0 1 2 3 4 5 6 7 8 9 10
0 10 20 30 40 50 60 70 80 90 100 110 120 130 140 150 160 170 180 190 200
Depth (m)
c

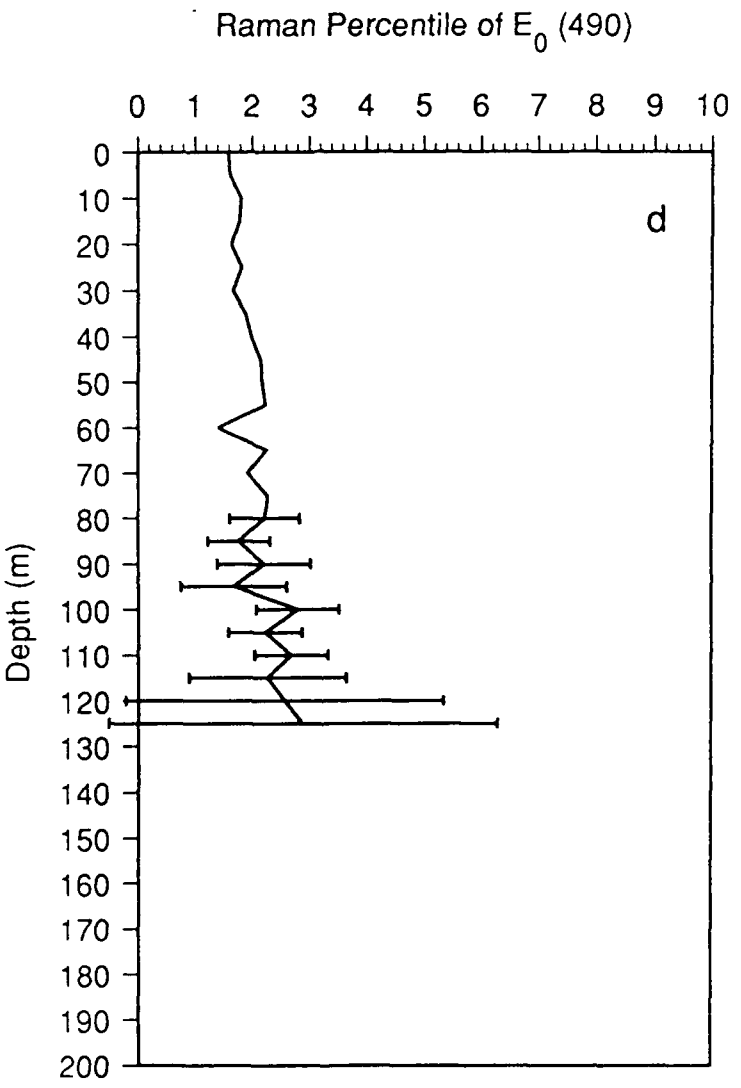
Raman Percentile of E_0 (490)
0 1 2 3 4 5 6 7 8 9 10
Depth (m)
0 10 20 30 40 50 60 70 80 90 100 110 120 130 140 150 160 170 180 190 200
d

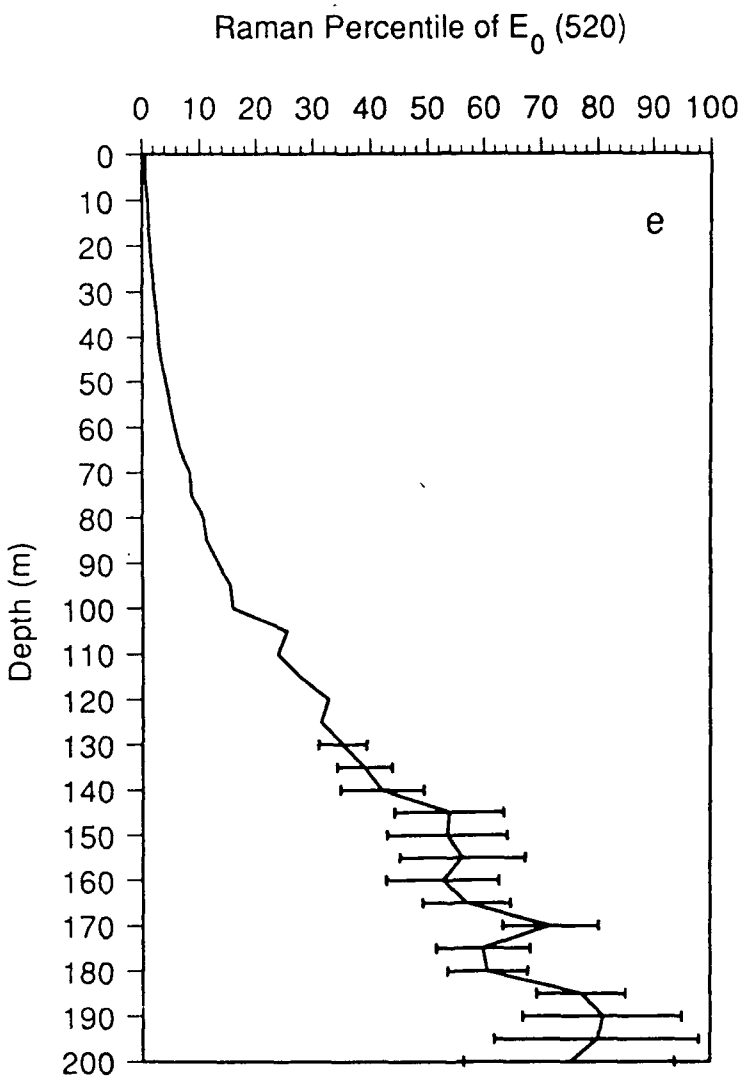
Raman Percentile of E_0 (520)
0 10 20 30 40 50 60 70 80 90 100
Depth (m)
0 10 20 30 40 50 60 70 80 90 100 110 120 130 140 150 160 170 180 190 200
e

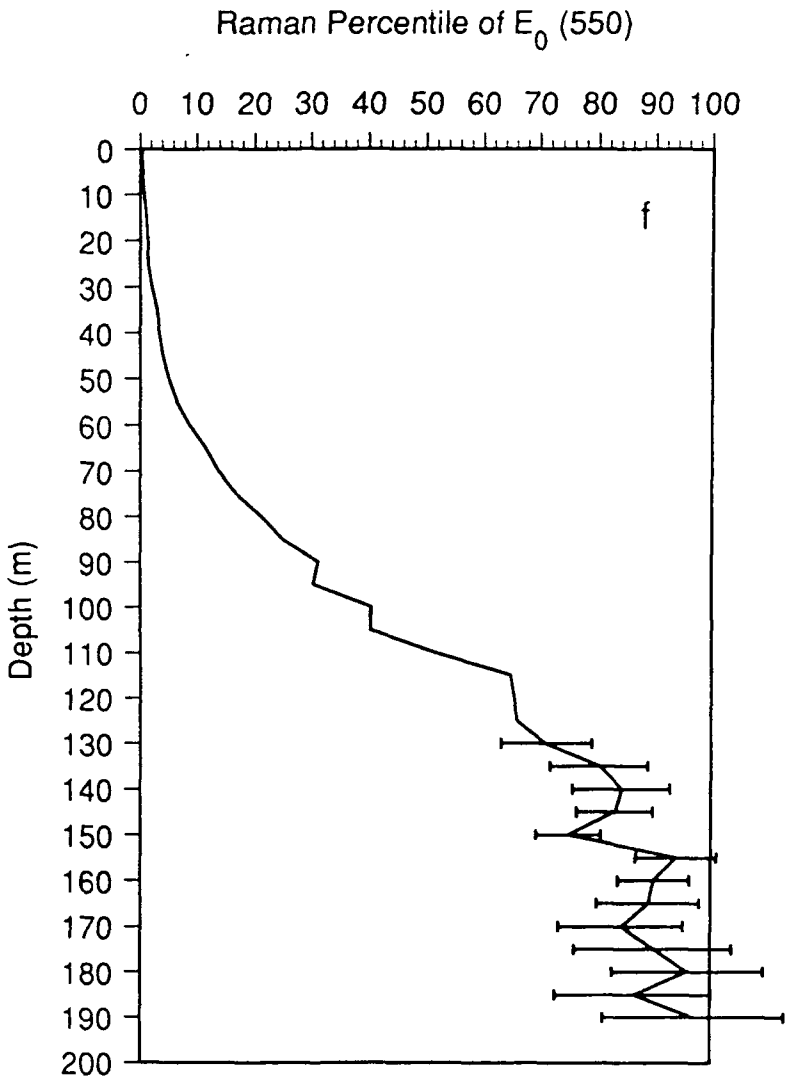
Raman Percentile of E_0 (550)
0 10 20 30 40 50 60 70 80 90 100
Depth (m)
0 10 20 30 40 50 60 70 80 90 100 110 120 130 140 150 160 170 180 190 200
f

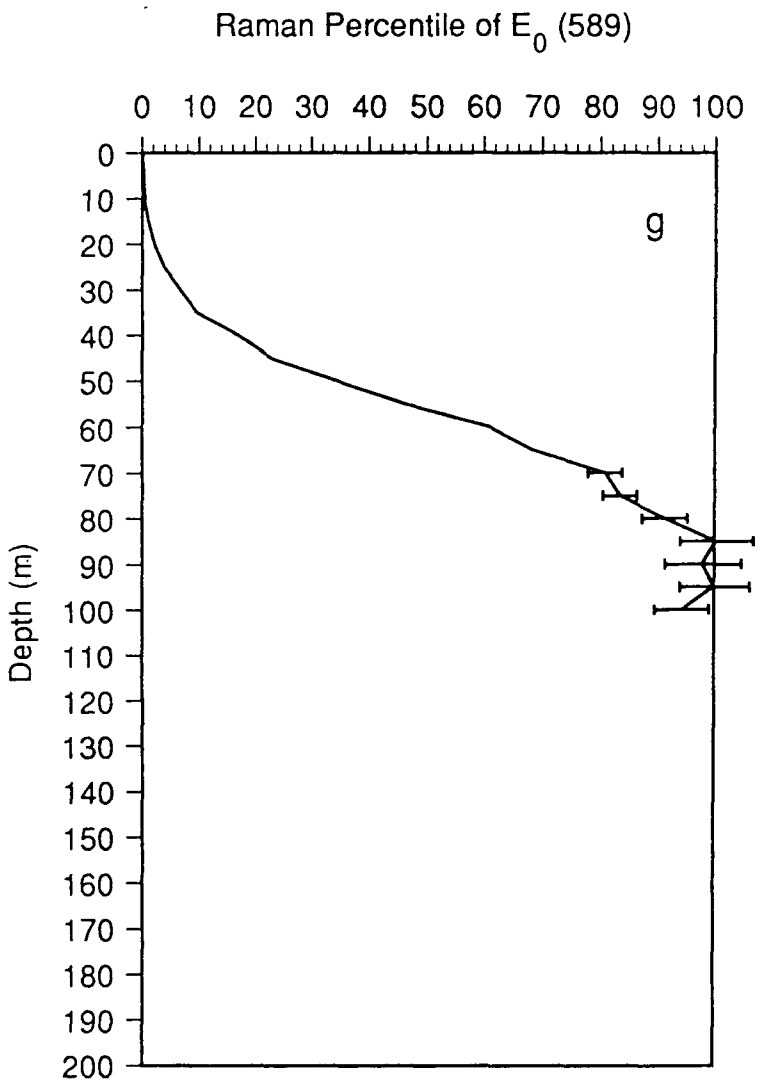
Raman Percentile of E_0 (589)
0 10 20 30 40 50 60 70 80 90 100
Depth (m)
0 10 20 30 40 50 60 70 80 90 100 110 120 130 140 150 160 170 180 190 200
g

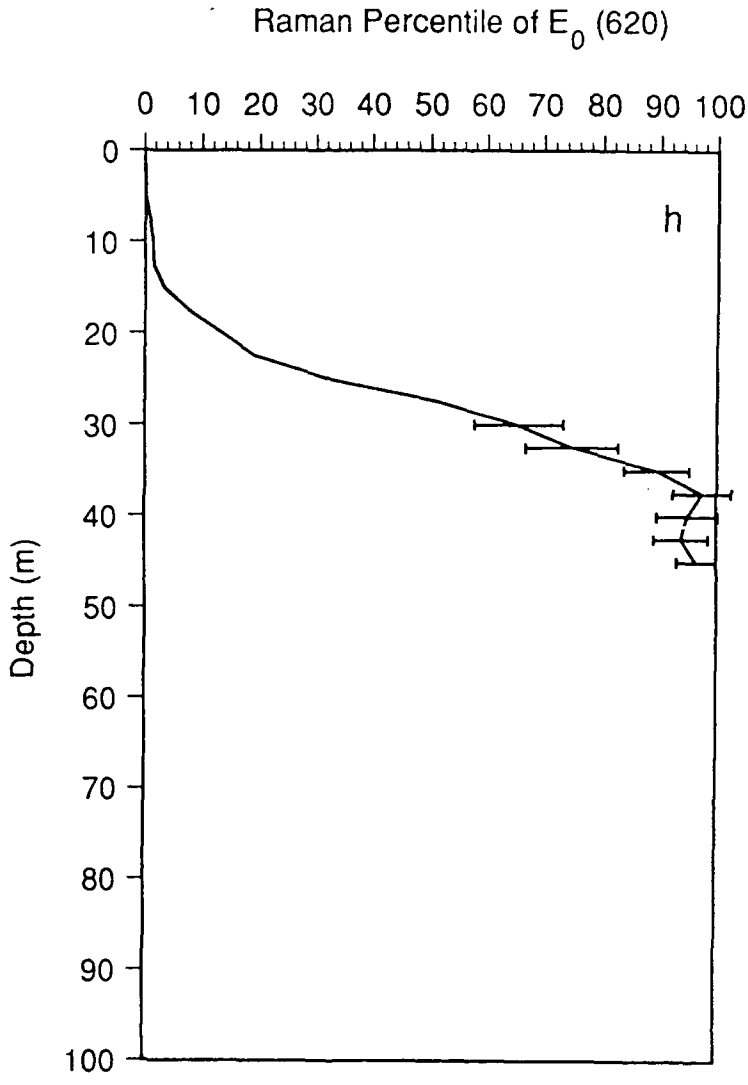
Raman Percentile of E_0 (620)
0 10 20 30 40 50 60 70 80 90 100
0
10
20
30
40
50
60
70
80
90
100
Depth (m)
h

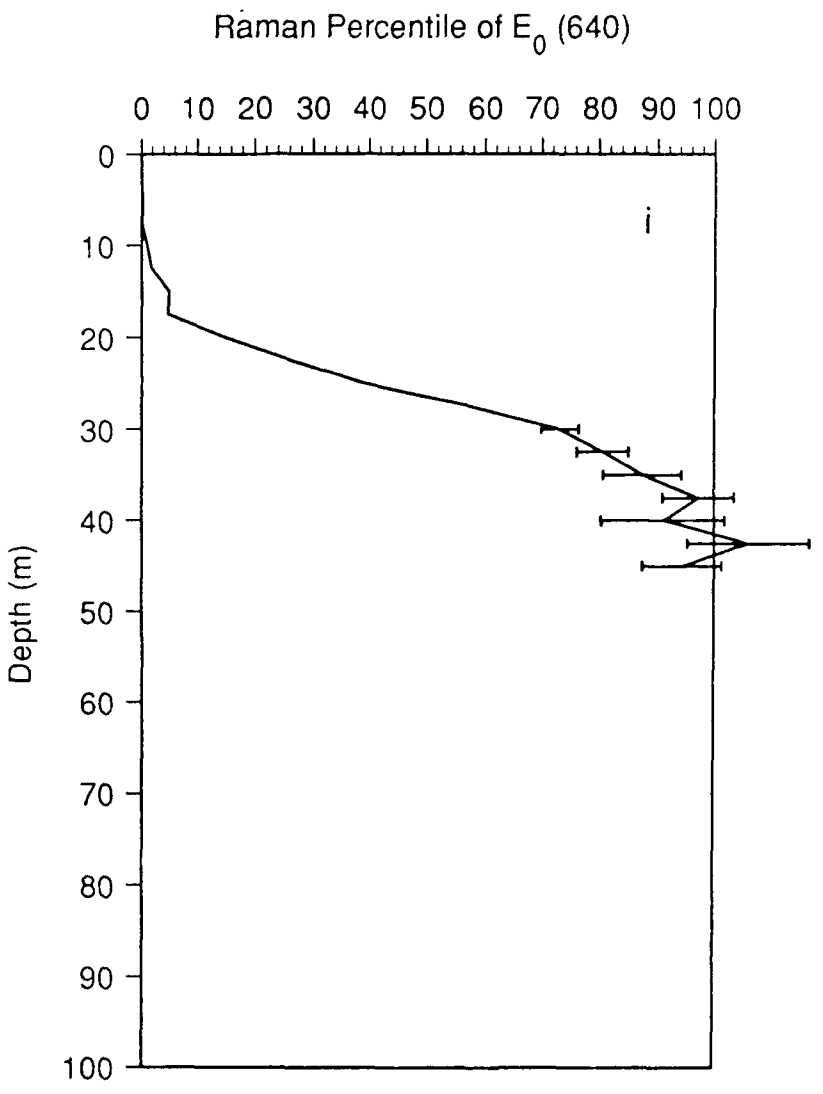
Raman Percentile of E_0 (640)
0 10 20 30 40 50 60 70 80 90 100
0
10
20
30
40
50
60
70
80
90
100
Depth (m)
i

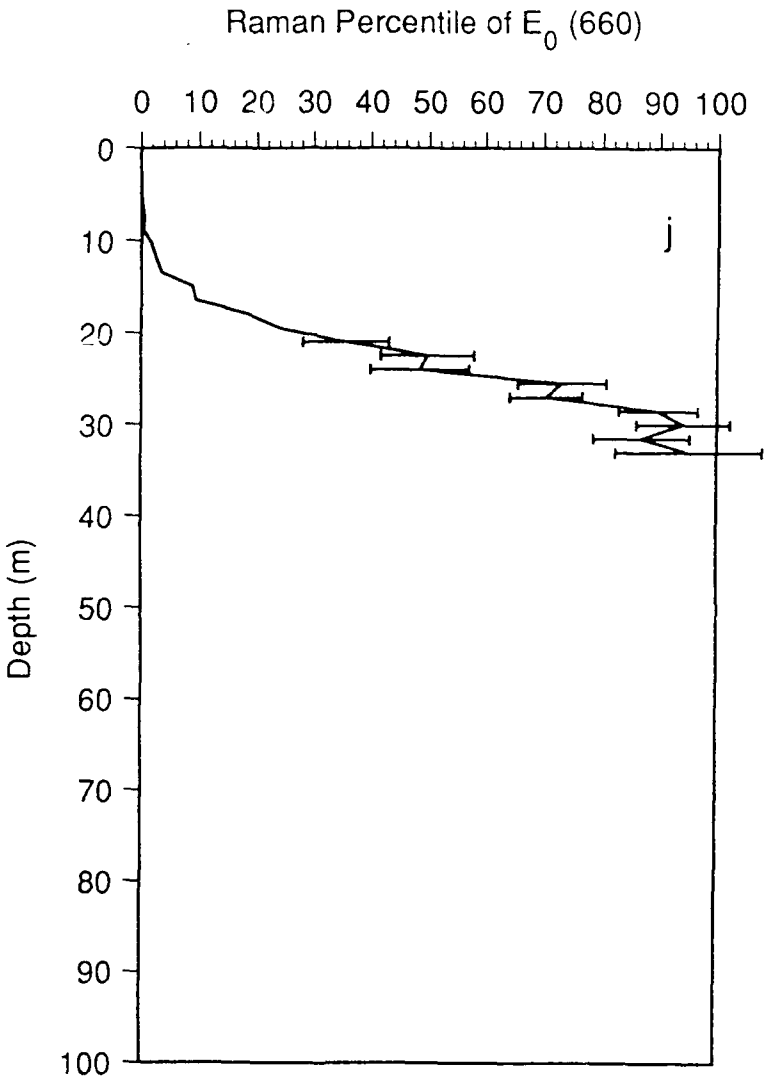
Raman Percentile of E_0 (660)
0 10 20 30 40 50 60 70 80 90 100
0
10
20
30
40
50
60
70
80
90
100
Depth (m)
j

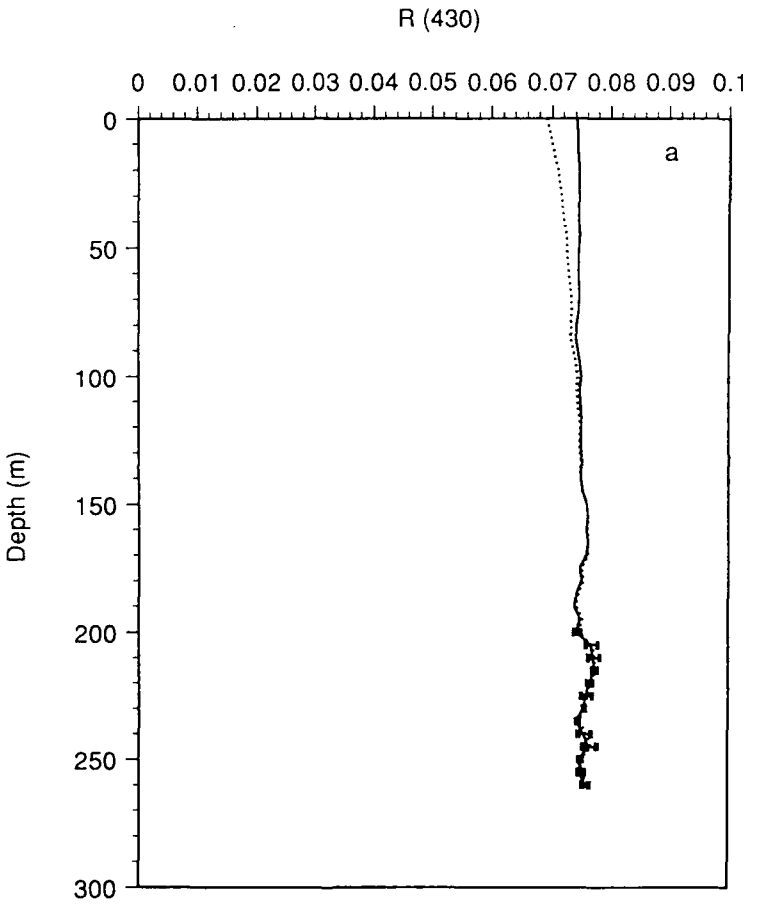
R (430)
0 0.01 0.02 0.03 0.04 0.05 0.06 0.07 0.08 0.09 0.1
0
50
100
150
200
250
300
Depth (m)
a

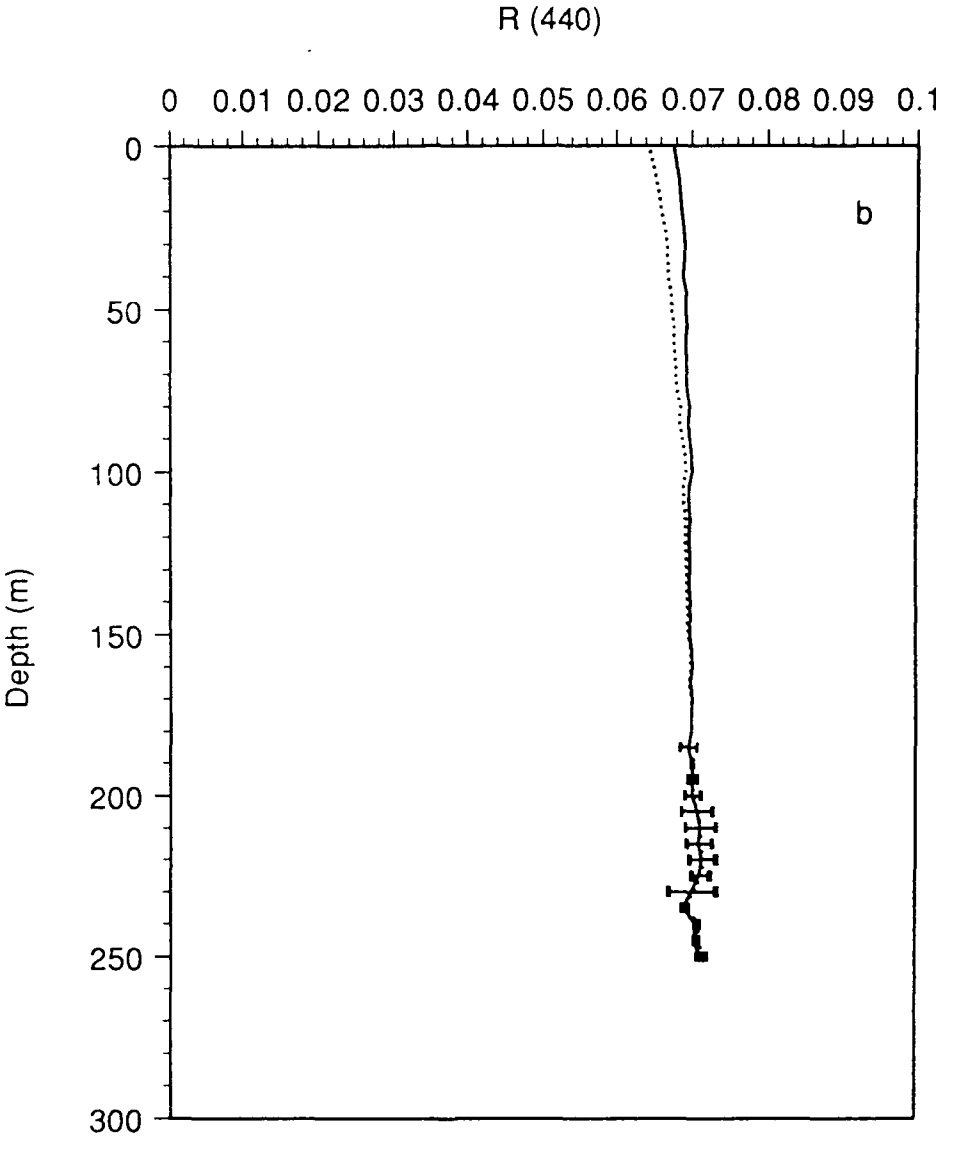
R (440)
0 0.01 0.02 0.03 0.04 0.05 0.06 0.07 0.08 0.09 0.1
0
50
100
150
200
250
300
Depth (m)
b

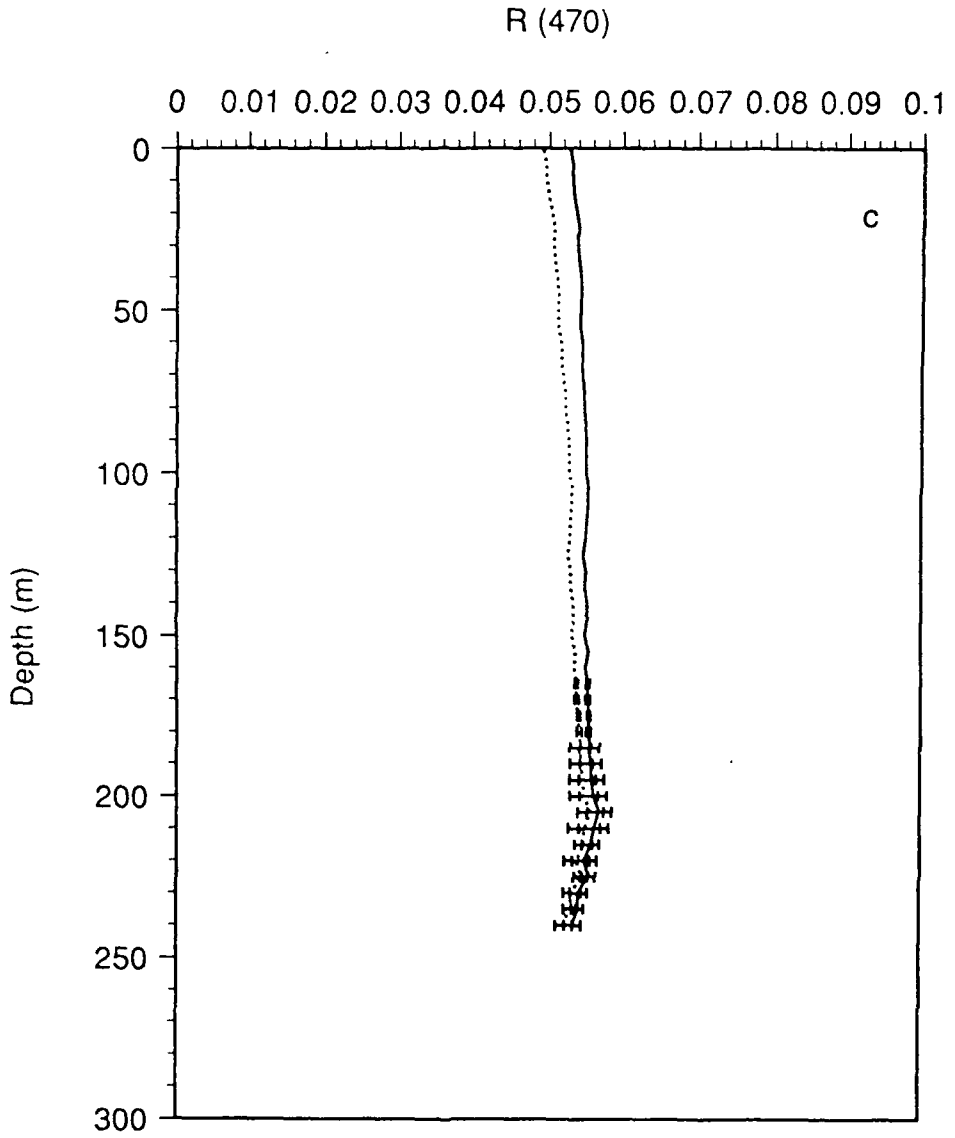
R (470)
0 0.01 0.02 0.03 0.04 0.05 0.06 0.07 0.08 0.09 0.1
0
50
100
150
200
250
300
Depth (m)
c

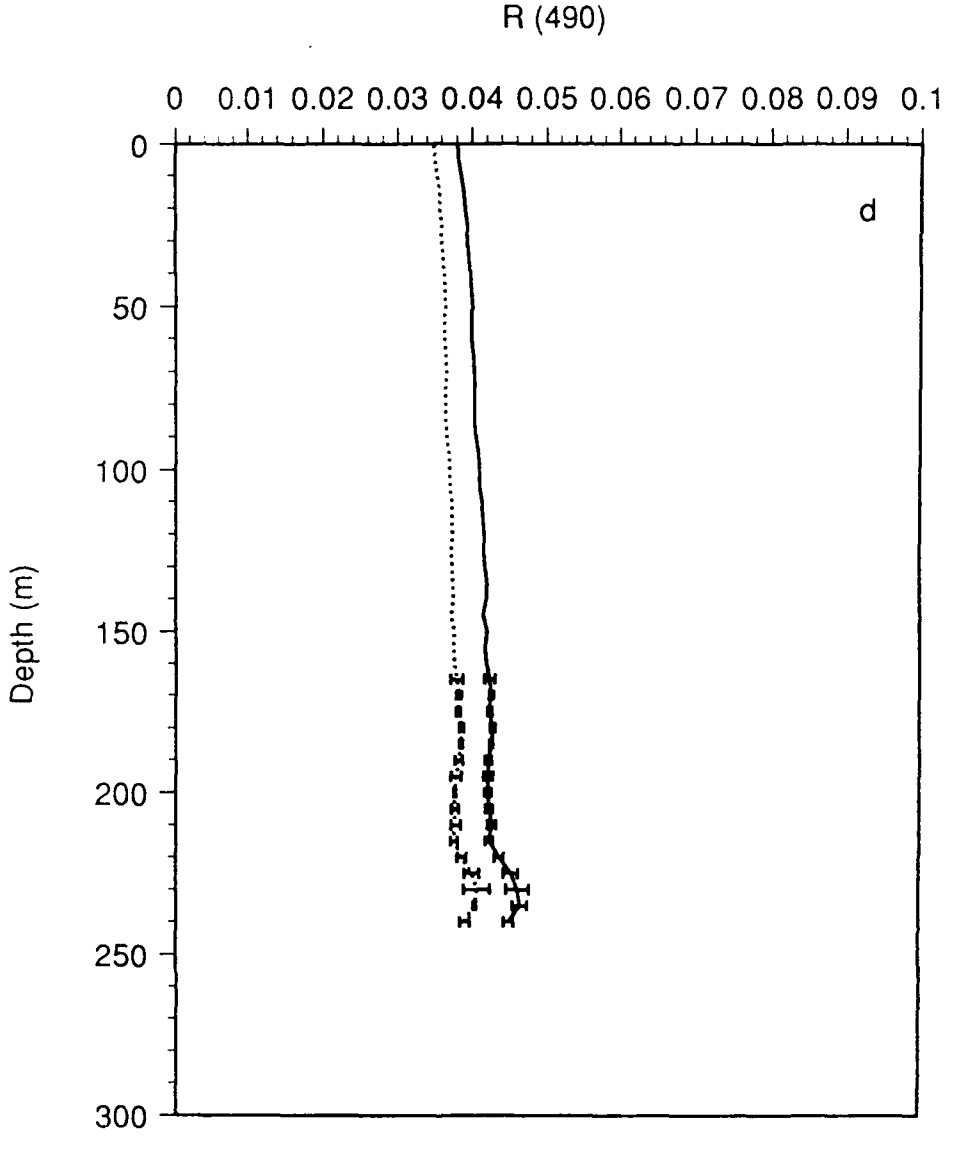
R (490)
0 0.01 0.02 0.03 0.04 0.05 0.06 0.07 0.08 0.09 0.1
0
50
100
150
200
250
300
Depth (m)
d

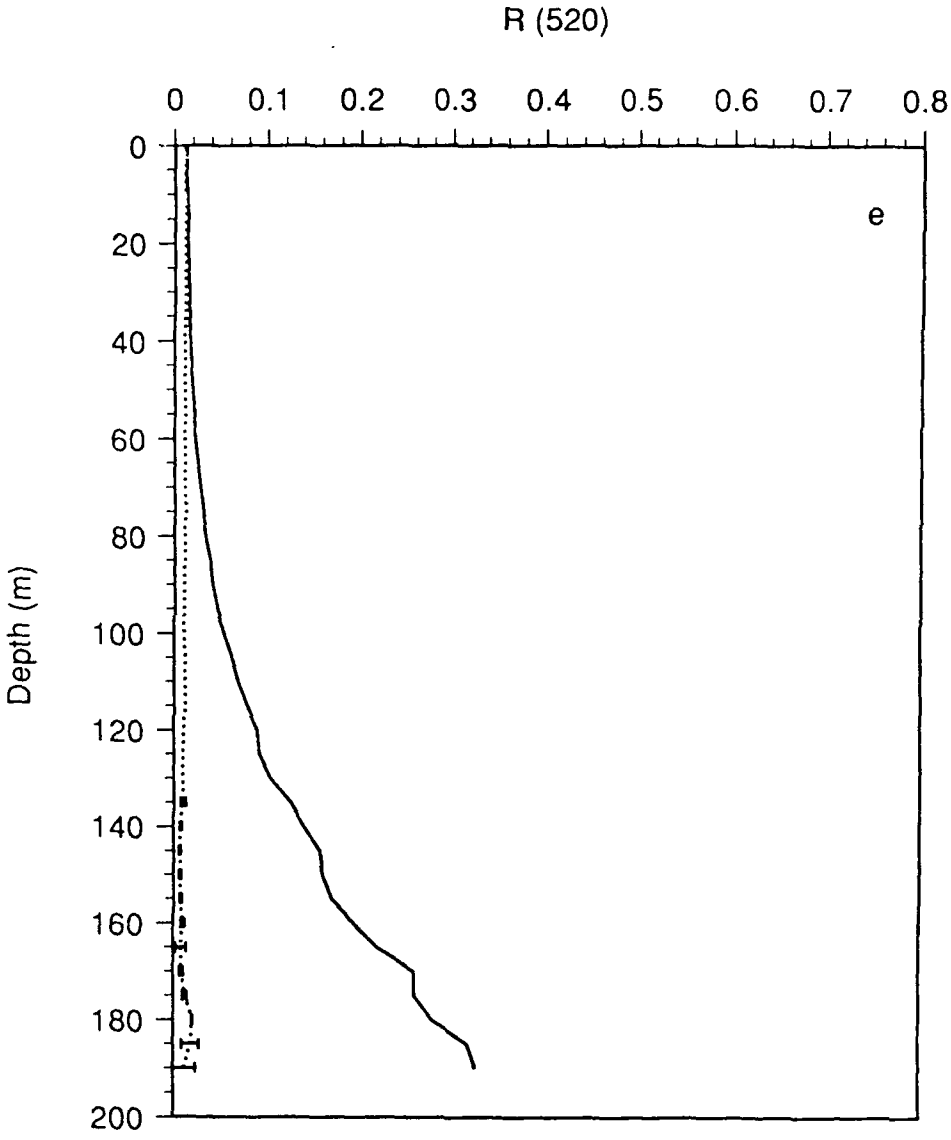
R (520)
0
0.1
0.2
0.3
0.4
0.5
0.6
0.7
0.8
0
20
40
60
80
100
120
140
160
180
200
Depth (m)
e

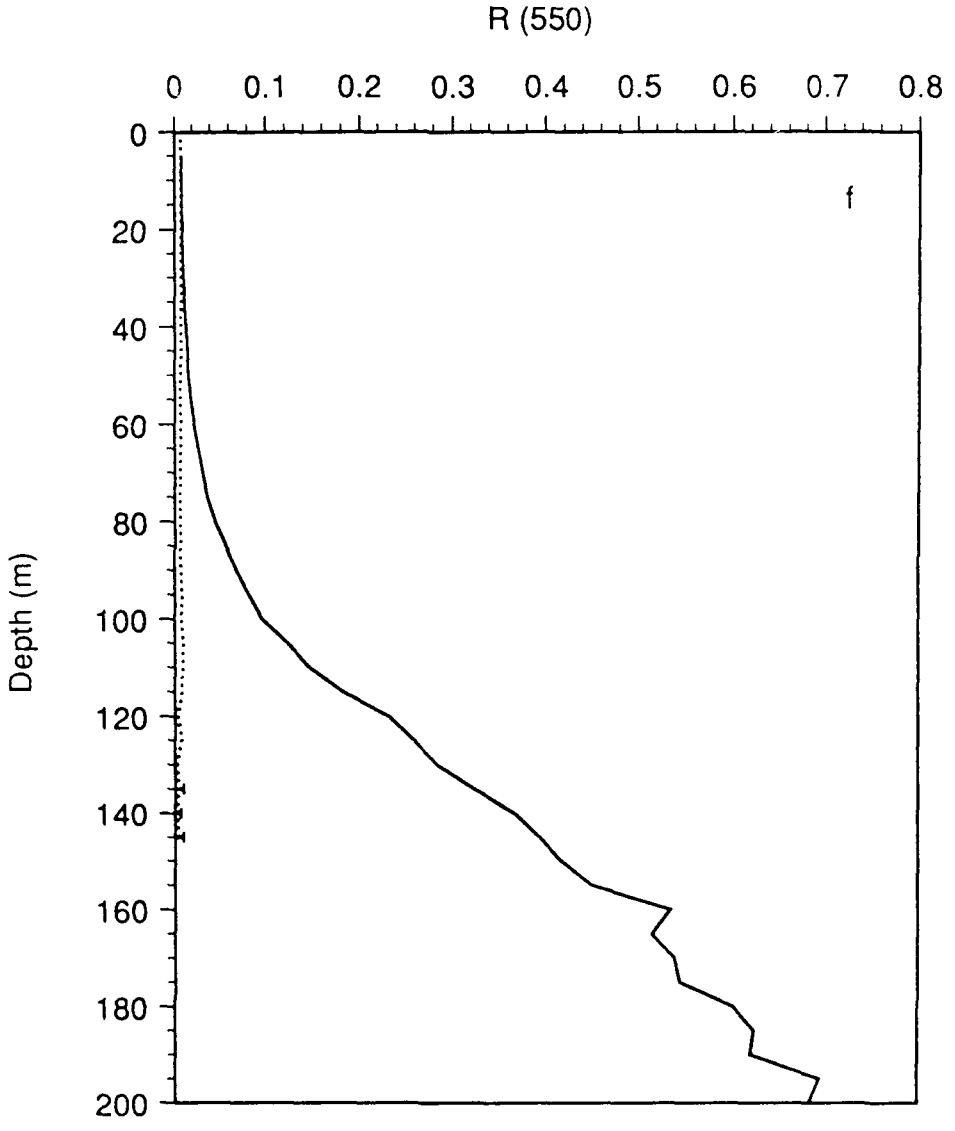
R (550)
0
0.1
0.2
0.3
0.4
0.5
0.6
0.7
0.8
0
20
40
60
80
100
120
140
160
180
200
Depth (m)
f

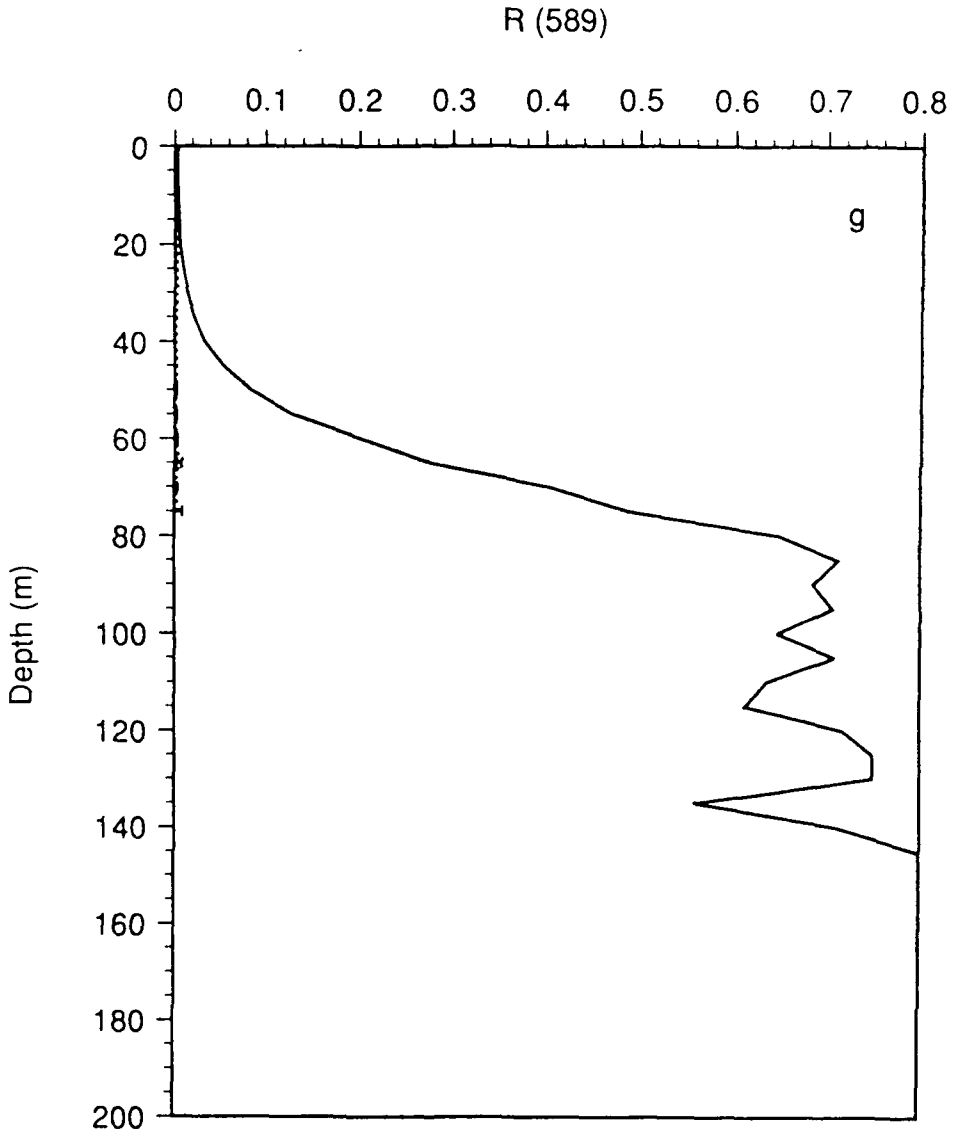
R (589)
0
0.1
0.2
0.3
0.4
0.5
0.6
0.7
0.8
0
20
40
60
80
100
120
140
160
180
200
Depth (m)
g

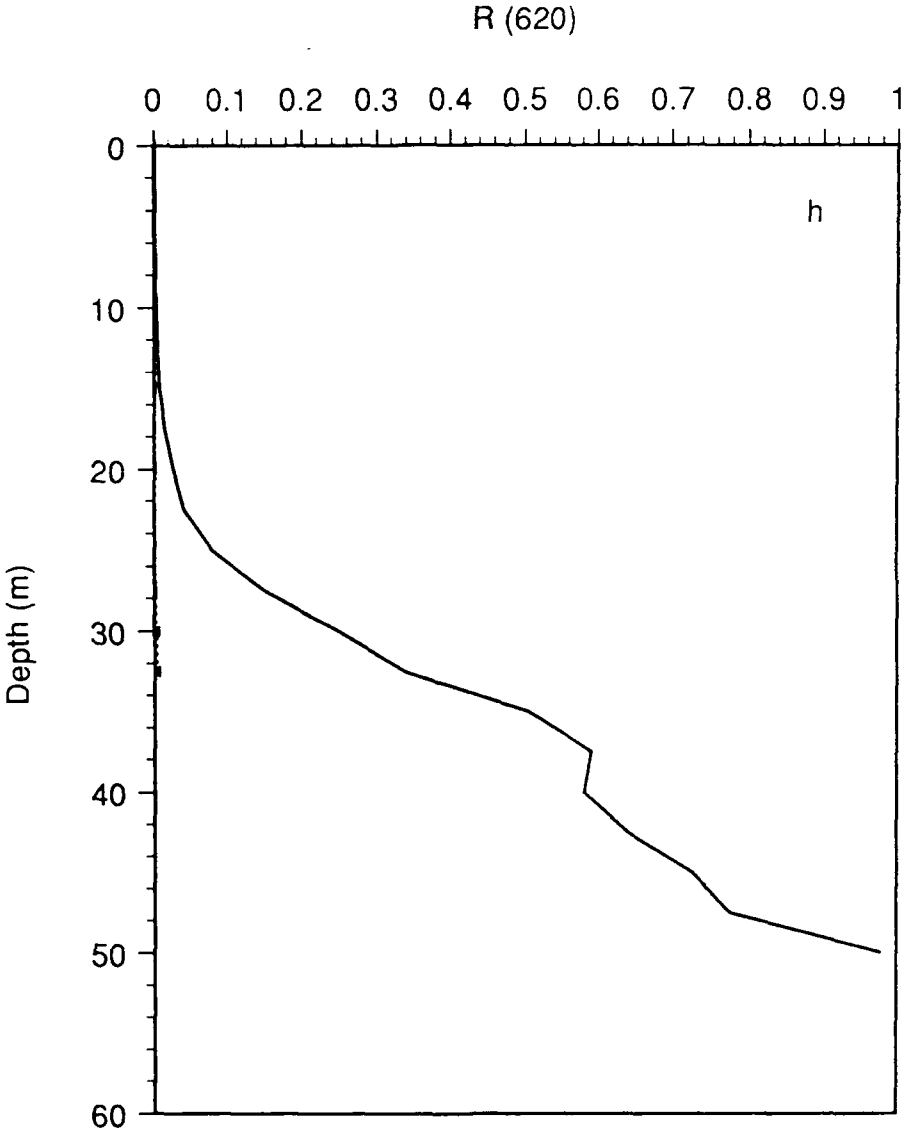
R (620)
0
0.1
0.2
0.3
0.4
0.5
0.6
0.7
0.8
0.9
1
0
10
20
30
40
50
60
Depth (m)
h

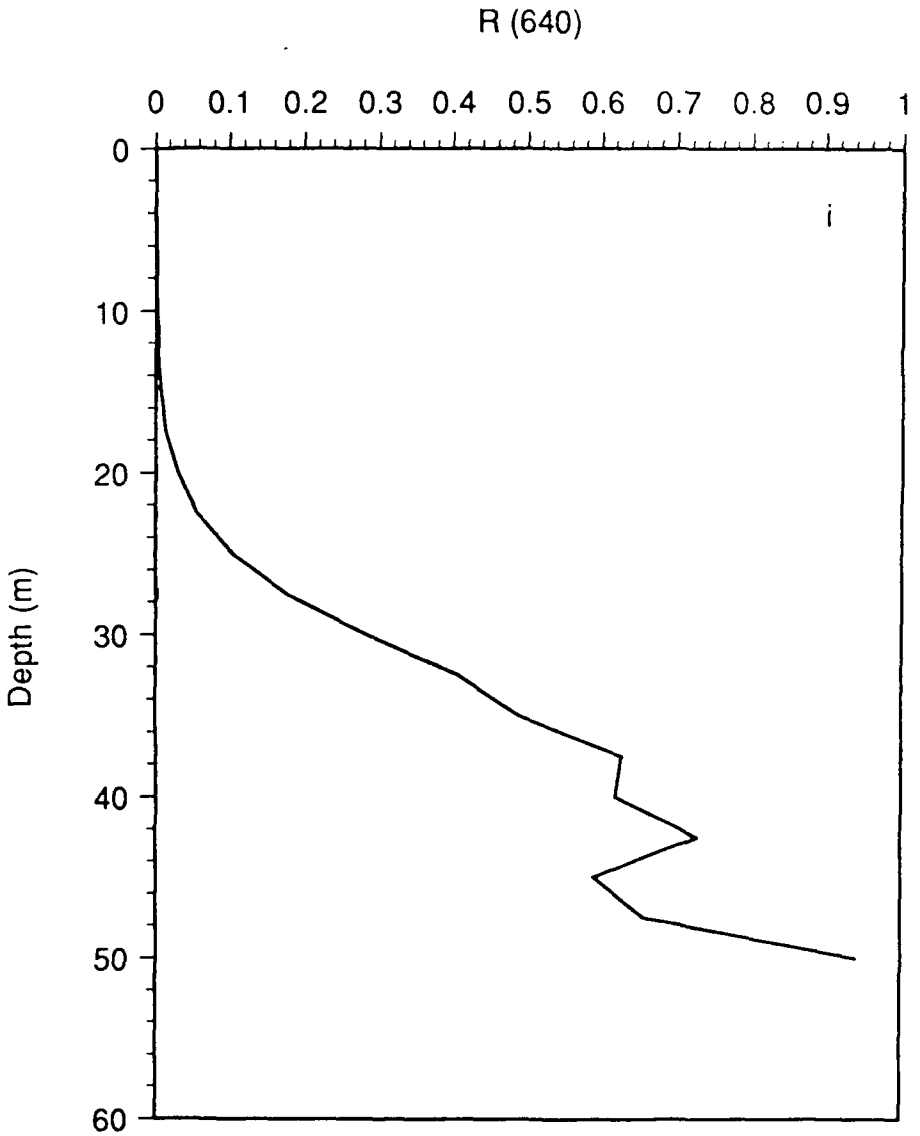
R (640)
0
0.1
0.2
0.3
0.4
0.5
0.6
0.7
0.8
0.9
1
0
10
20
30
40
50
60
Depth (m)

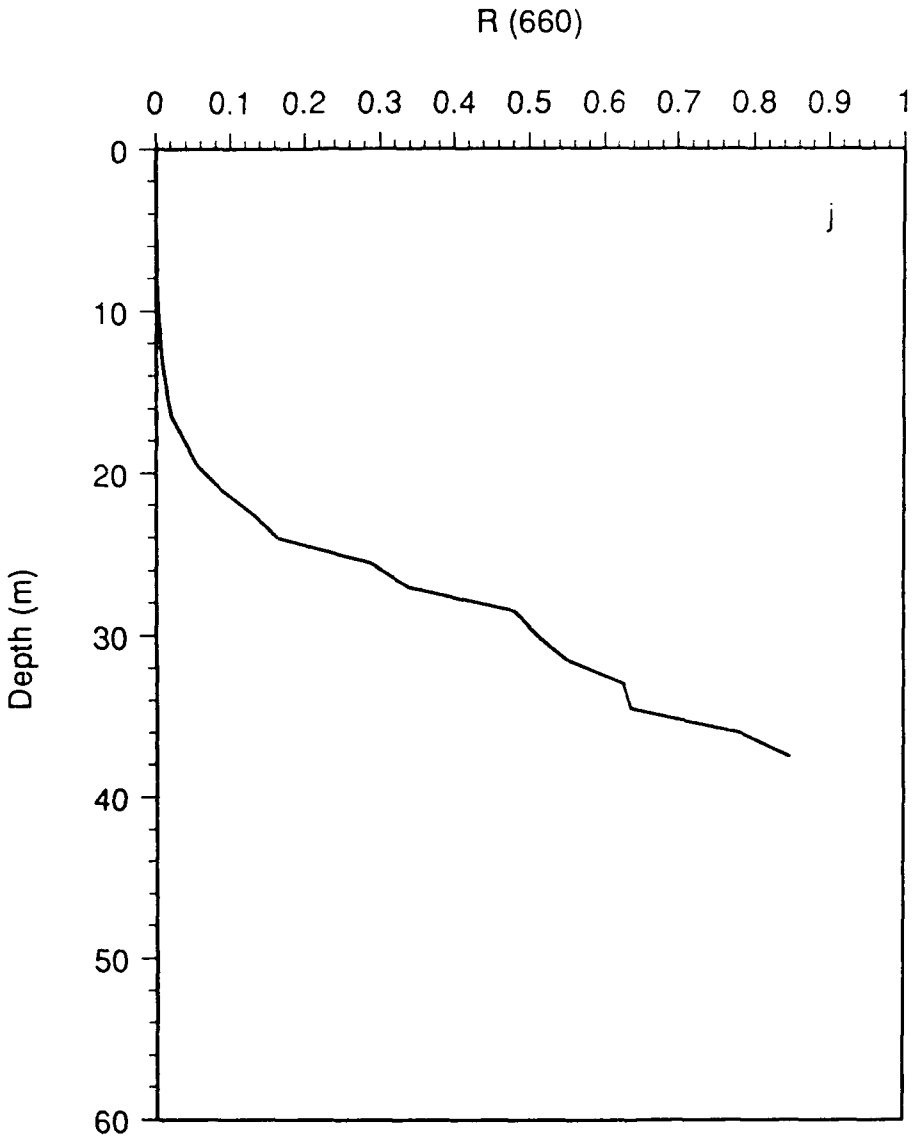
R (660)
0
0.1
0.2
0.3
0.4
0.5
0.6
0.7
0.8
0.9
1
Depth (m)
0
10
20
30
40
50
60
j

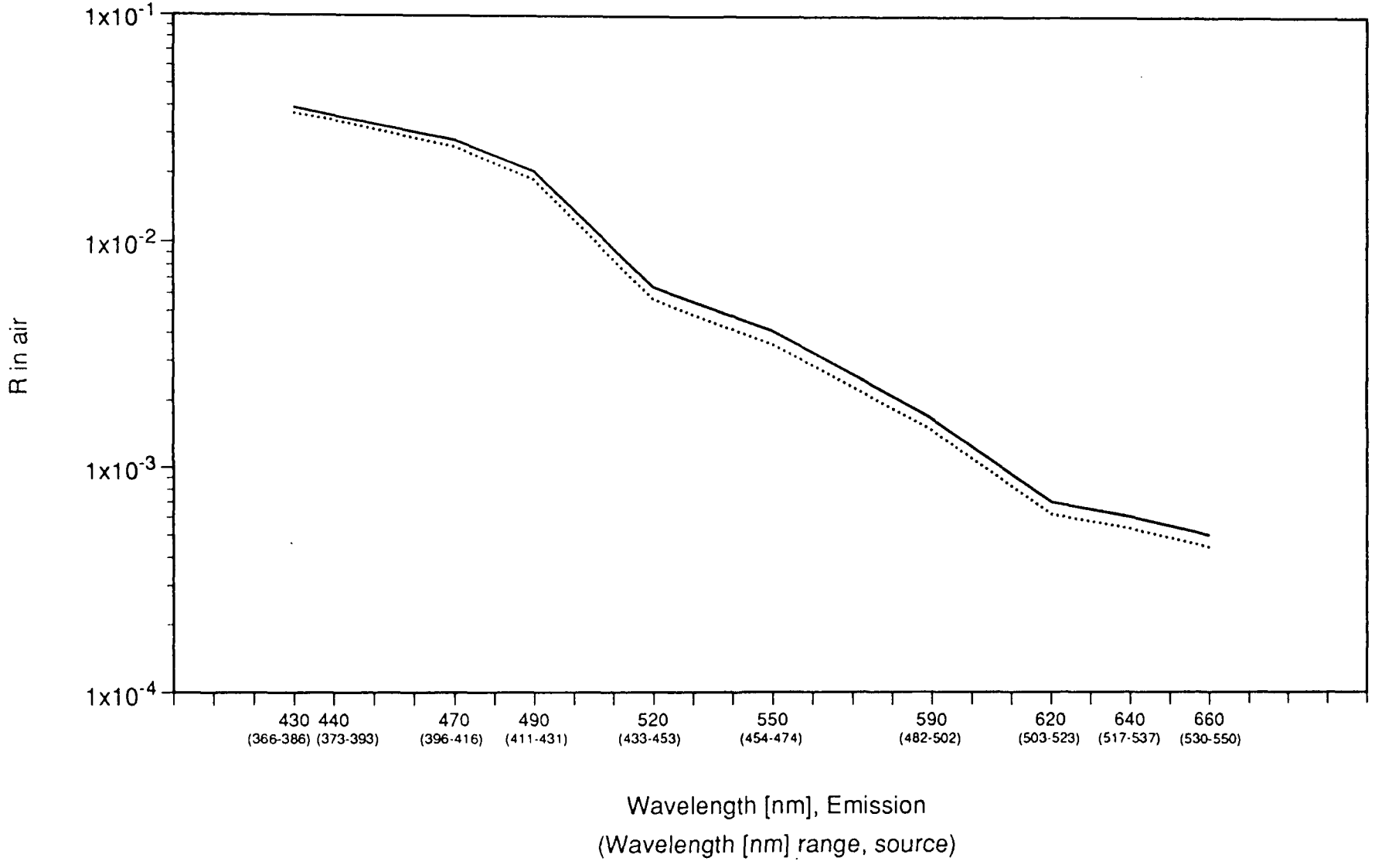
1x10-1
1x10-2
1x10-3
1x10-4
R in air
430 440
(366-386) (373-393)
470
(396-416)
490
(411-431)
520
(433-453)
550
(454-474)
590
(482-502)
620
(503-523)
640
(517-537)
660
(530-550)
Wavelength [nm], Emission
(Wavelength [nm] range, source)

INITIAL DISTRIBUTION LIST

	ADDRESSEES	NUMBER OF COPIES
1.	Scientific Officer Code 1123OP Dr. Gary Gilbert Office of Naval Research 800 North Quincy Street Arlington, VA 22217-5000	3
2.	Director, Naval Research Laboratory Attn: Code 1001 Washington, DC 20375	1
3.	Defense Technical Information Center Bldg. 5, Cameron Station Alexandria, VA 22314	12
4.	Naval Research Laboratory Stennis Space Center, MS 39529-5004 Dr. Albert W. Green, Jr. Code 7330	1
5.	Naval Research Laboratory 4555 Overlook Ave., SW Washington, DC 20375 Dr. Eric Hartwig, Code 7000	1